12-2002

Geochemical and Isotopic Characteristics Associated with High Conductivities in a Shallow Hydrocarbon-Contaminated Aquifier

Franklyn D. Legall
Western Michigan University

GEOCHEMICAL AND ISOTOPIC CHARACTERISTICS ASSOCIATED WITH HIGH CONDUCTIVITIES IN A SHALLOW HYDROCARBON-CONTAMINATED AQUIFER

by

Franklyn D. Legall

A Dissertation
Submitted to the
Faculty of The Graduate College
in partial fulfillment of the
requirements for the
Degree of Doctor of Philosophy
Department of Geosciences

Western Michigan University
Kalamazoo, Michigan
December 2002

ACKNOWLEDGEMENTS

The author would like to thank Dr. Estella Atekwana for her unwavering support, guidance, and encouragement towards the completion of this study. Special thanks to Dr. Eliot Atekwana for many hours of useful discussions and his assistance with field logistics and sampling, and for providing laboratory facilities at Indiana University-Purdue University Indianapolis (IUPUI) for the geochemical analyses and CO_2 extraction for isotope analyses. Appreciation is also expressed to the other members of my supervisory committee, including Dr. R.V. Krishnamurthy and Dr. William Sauck for their assistance and supervision during the course of this study.

I would like to thank Douglas D. Werkema for supplying the soil conductivity data that was integral to this study, and Jennifer Latimer at IUPUI for conducting the metal analysis. DLZ Michigan, Inc. generously provided logistical support, including Geoprobe® services for the installation of sampling equipment, and computer-aided drafting (CAD) assistance. I thank my family and friends for their support.

Partial funding for this study was provided by the American Petroleum Institute-National Ground Water Association (API/NGWA), the National Aeronautics and Space Administration through the Michigan Space Grant Consortium, and the American Chemical Society-Petroleum Research Fund Grant (PRF# 31594-AC2).

This dissertation is dedicated to the memory of my mother, Elmina Legall.

Franklyn D. Legall

GEOCHEMICAL AND ISOTOPIC CHARACTERISTICS ASSOCIATED WITH HIGH CONDUCTIVITIES IN A SHALLOW HYDROCARBON-CONTAMINATED AQUIFER

Franklyn D. Legall, Ph.D.

Western Michigan University, 2002

In-situ vertical resistivity probes (VRPs) deployed at a hydrocarbon-contaminated site in SW Michigan showed high soil conductivities within the contaminated zone. Within this zone, different phases of hydrocarbon impact were recognized, namely, zones with residual and dissolved phase hydrocarbons (RDH) and zones where these phases coexist with free product (RDFH). Bulk soil conductivities were highest (12 to 30 mS/m) in the zone with RDFH compared to the RDH zone (10 to 25 mS/m). Groundwater chemistry and stable carbon isotope data from closely spaced vertical samples within the anomalous conductive zones were used to provide evidence for biodegradation and to investigate the role of mineral weathering in the aquifer as the source of ions responsible for the observed conductivities.

Depth distribution of TEAs and educts showed evidence of reduction of nitrate, iron, manganese, and sulfate across steep vertical gradients. Within the zone with RDH, the reduction of NO_3, Fe (III), Mn(IV), and SO_4 were the major observed redox processes. This zone also exhibited the highest DIC. The $\delta^{13}C_{DIC}$ values of

–16.9 to –9.5‰ suggest that DIC evolution in this zone is controlled by carbonate dissolution through enhanced CO_2 production related to microbial hydrocarbon degradation. Within the zone with RDFH, DIC was lower compared to the RDH location with an associated $\delta^{13}C_{DIC}$ in the range of +6.5 to –4.4‰. Both the DIC and $\delta^{13}C_{DIC}$ suggest that methanogenesis is the dominant redox process.

The results also show higher concentrations of Na, Ca, and Mg associated with high soil conductivities in the contaminated portion of the aquifer compared to background that is consistent with the weathering of carbonate and Na and Ca feldspars, the dominant minerals in the aquifer. This ion enrichment translated to higher TDS at the contaminated locations as reflected in the conductivity measurements. The results suggest an interrelationship between redox processes, biomineralization of hydrocarbons, and high soil conductivities. Moreover, bulk conductivity measurements may be useful in assessing the potential for natural attenuation in contaminated, unconsolidated, sandy aquifers.

TABLE OF CONTENTS

Table of Contents—continued

CHAPTER

Table of Contents—continued

CHAPTER

LIST OF TABLES

Chapter II

Chapter III

LIST OF FIGURES

Chapter II

Chapter III

List of Figures--continued

CHAPTER I

INTRODUCTION

The high cost of engineered cleanups of many sites contaminated by light non-aqueous phase liquids (LNAPLs) has led to the proposal and acceptance of risk-based strategies and programs to facilitate environmental cleanups (ASTM, 1994; 1995; 2000). This risk-based approach to corrective action relies on an understanding of the geochemical and microbial processes that result in the intrinsic bioremediation of petroleum contaminants in the subsurface. Current methods of evaluating intrinsic bioremediation in the field rely heavily on monitoring strategies that are required to demonstrate that natural attenuation is occurring and to detect changes in hydrologic, geochemical, and microbiological conditions that may affect the efficacy of the natural attenuation process (Wiedemeier et al., 1995; Wiedemeier et al., 1998; Wiedemeier et al., 1999; Wiedemeier and Haas, 2002).

Techniques presently employed for monitoring intrinsic hydrocarbon degradation in field settings rely on direct sampling of soil and groundwater and their subsequent analysis to provide geochemical and microbiological data to interpret degradation activities. However, direct soil and groundwater sampling and analyses are often expensive and significant cost reductions may only be realized during the long term monitoring phase of the project (Wiedemeier and Haas, 2002). Another problem with this approach is the selection of sampling locations, because, to a large

extent, the placement of sample collection points and the subsurface intervals selected for characterization are arbitrary and may not provide the spatial resolution necessary to assess contaminant distribution or its degradation. A possible solution to this problem may lie with combining geochemical and geophysical investigations.

A number of recent studies (Sauck et al., 1998; Atekwana et al., 2000; Werkema, 2002) have documented high conductive zones in soils extending from the top of the hydrocarbon-impacted zone into the saturated zone. On this basis, Sauck et al. (1998) and Atekwana et al. (2000) have proposed a model linking the higher soil conductivities to LNAPL biodegradation. Their model suggests that the hydrocarbon plume characteristics change over time from initially resistive to more conductive as LNAPL undergo microbial degradation. Microbial degradation of hydrocarbons produces acids that increase the weathering properties of the pore fluids. Water-rock reactions alter the aquifer minerals and lead to an enrichment of ions in the groundwater. Higher bulk conductivities associated with soils in which hydrocarbon biodegradation is occurring are attributed to the higher ionic strength of the pore fluids.

The relationship between bulk soil conductivity and geochemical characteristics associated with an aged hydrocarbon plume was investigated at an abandoned refinery site located in Carson City, Michigan. Spatial and temporal variations in soil conductivity within the hydrocarbon-contaminated zone, and the role of water level fluctuations on the soil conductivity have been investigated using a network of vertical resistivity probes (VRPs) installed at the site (Werkema, 2002).

Furthermore, previous studies (Duris et al., 2000; Werkema et al., 2000) have demonstrated a possible link between high soil conductivity and the distribution of hydrocarbon degrading bacteria. Extensive evidence exists in the literature for mineral weathering in contaminated aquifers. There is general consensus that the breakdown of carbonate and silicate minerals by organic acids produced during microbial hydrocarbon degradation is far more effective than by carbonic acid (Hiebert and Bennett, 1992; Welch and Ullman, 1993; McMahon et al., 1995; Ullman and Welch, 2002). However, in order to establish that the high soil conductivities are indeed due to the biomineralization of hydrocarbons there is the need to demonstrate such evidence by examining the geochemical processes occurring in the subsurface, and documenting the products of the resulting mineral-water reactions in the aquifer that may account for the soil conductivity anomalies.

Therefore the focus of the study was: (a) to take advantage of the zonations afforded by the resistivity surveys to more closely investigate the redox processes within the aquifer and provide geochemical evidence of biodegradation, (b) to document in a field setting how vertical changes in the groundwater chemistry (major ions, DIC, and stable isotopes) co-vary with bulk conductivity in contaminated and uncontaminated groundwater, and (c) to assess the contribution of major ions derived from mineral-water reactions that result from geochemical and biogeochemical processes which modify the aquifer matrix sufficiently to alter the bulk soil conductivity.

The coupling of high resolution soil conductivity measurements with geochemical and isotopic data from closely spaced vertical sampling provides the

basis for examining the link between the geochemical changes related to microbial hydrocarbon biodegradation, and changes in the bulk soil conductivity at contaminates sites. The work contained in this thesis represents a first attempt to systematically test the hypothesis that weathering of aquifer minerals that occur during microbial degradation of hydrocarbons provides the ions in solution to alter the bulk conductivity of soils.

References

American Society for Testing and Materials (ASTM), 1994. Emergency Standard Guide for Risk-Based Corrective Action Applied at Petroleum Release Sites, ES 38-94.

American Society for Testing and Materials (ASTM), 1995. Standard Guide for Risk-Based Corrective Action Applied at Petroleum Release Sites, E1739-95.

Atekwana, E. A., Sauck, W. A. and Werkema, D. D., 1998. Characterization of a complex refinery groundwater contamination plume using multiple geoelectric methods. Symposium on the Application of Geophysics to Environmental and Engineering Problems. Chicago, IL.

Atekwana, E. A., Sauck, W. A. and Werkema, D. D., 2000. Investigations of geoelectrical signatures at a hydrocarbon contaminated site. J Appl. Geophys. 44, 167-180.

Duris, J. W., Werkema, D. D., Atekwana, E. A., Eversole, R., Beuving, L. and Rossbach, S., 2000. Microbial communities and their effects on silica structure and geophysical properties in hydrocarbon impacted sediments. Geological Society of America Program with Abstracts, 32. A-190.

Hiebert, F. K. and Bennett, P. C., 1992. Microbial control of silicate weathering in organic-rich groundwater. Science, 258. 278-281.

McMahon, P. B. Vroblesky, D. A., Bradley, P. M., Chapelle, F. H. and Gullet, C. D., 1995. Evidence for enhanced mineral dissolution in organic acid-rich shallow groundwater. Ground Water, 33. 207-216.

Sauck, W. A., 2000. A conceptual model for the geoelectrical response of LNAPL plumes in granular sediments. J. Appl. Geophys, 44. 151-165.

Sauck, W. A., Atekwana, E. A. and Nash, M. S., 1998. Elevated conductivities associated with an LNAPL plume imaged by integrated geophysical techniques. J. Environ. Eng. Geophys., 2-3. 203-212.

Ullman, W.J. and Welch, S. A., 2002. Organic ligands and feldspar dissolution. In: R. Hellmann and S. A. Ward (Editors): Water-rock interactions, ore-deposits, and environmental geochemistry-A tribute to David A. Crerar. The Geochemical Society Special Publication No. 7.

Welch, S.A. and Ullman, W. J., 1993. The effects of organic acids on plagioclase dissolution rates and stoichiometry. Geochim. Cosmochim. Acta., 57. 2725-2736.

Werkema D. D., Atekwana, E. A., Sauck, W. A., Rossbach, S. and Duris, J., 2000. Vertical distribution of microbial abundances and apparent resistivity at an LNAPL spill site. Proceedings of the Symposium on the Application of Geophysics to Engineering and Environmental Problems (SAGEEP), Arlington Virginia, 669-678.

Werkema, D. D., 2002. Geoelectrical response of an aged LNAPL plume: Implications for monitoring natural attenuation. (Unpublished Ph.D. Thesis, Western Michigan University, Kalamazoo, MI).

Wiedemeier, T. H., Wilson, J. T., Kampbell, D. H., Miller, R. N. and Hansen, J. E., 1995. Technical protocol for implementing intrinsic remediation with long term monitoring for natural attenuation of fuel contamination dissolved in groundwater. San Antonio, Texas: U.S. Air Force Center for Environmental Excellence.

Wiedemeier, T. H., Swanson, M. A., Moutoux, D. E., Gordon, E. K., Wilson, J. T., Wilson, B. H., Kampbell, D. H., Haas, P. E., Miller, R. N., Hansen, J. E. and Chapelle, F. H., 1998. Technical protocol for evaluating natural attenuation of chlorinated solvents in groundwater. EPA/600/R-98/128:ftp://ftp.epa.gov. pub/ada/reports/protocol.pdf.

Wiedemeier, T. H., Rifai, H. W., Newell, C. J. and Wilson, J. T., 1999. Natural attenuation of fuels and chlorinated solvents in the subsurface. New York: John Wiley and Sons.

Wiedemeier, T. H. and Haas, P.E., 2002. Designing monitoring programs to effectively evaluate the performance of natural attenuation. Ground Water Monitoring and Remediation, 22(3): 124-134.

CHAPTER II

GEOCHEMICAL AND ISOTOPIC CHARACTERISTICS ASSOCIATED WITH HIGH CONDUCTIVITIES IN A SHALLOW HYDROCARBON-CONTAMINATED AQUIFER: I. EVIDENCE FOR HYDROCARBON DEGRADATION

Abstract

Geochemical and isotopic data from closely spaced vertical samples within high conductive soils zones in a shallow hydrocarbon-impacted aquifer were used to provide geochemical evidence for biodegradation and to investigate redox processes occurring within the conductive zones. The aquifer is contaminated by dissolved and residual phase hydrocarbons (RDH) as well as dissolved, residual and free phase hydrocarbons (RDFH). Bulk soil conductivities were highest (12 to 30 mS/m) in the RDFH zone compared to the RDH zone (10 to 25 mS/m).

Evidence of microbial hydrocarbon degradation was assessed by measurements of terminal electron acceptors (TEAs) NO_3 and SO_4 and educts NH_4, Fe(II), Mn(II), dissolved inorganic carbon (DIC), alkalinity, and the isotopic ratio of DIC ($\delta^{13}C_{DIC}$). Depth distribution of TEAs and educts showed evidence of reduction of nitrate, iron, manganese, and sulfate across steep vertical gradients.

Within the portion of the plume characterized by RDH, SO_4 reduction has supplanted denitrification via dissimilatory nitrate reduction, and the reduction of Fe (III) and Mn(IV) as the major observed redox process. The highest DIC values were

reported in this zone. The $\delta^{13}C_{DIC}$ values of –16.9 to –9.5‰ suggest that DIC evolution within this zone is controlled by carbonate dissolution through enhanced CO_2 production related to microbial hydrocarbon degradation.

Within the portion of the aquifer with RDFH, DIC was lower compared to the RDH location with an associated $\delta^{13}C_{DIC}$ in the range of +6.5 to –4.4‰. Both the DIC and $\delta^{13}C_{DIC}$ suggest that methanogenesis is the dominant redox process. The present study provides a qualitative assessment of the interrelationship between redox processes, biomineralization of hydrocarbons, and high bulk soil conductivities.

Introduction

In-situ soil investigations at hydrocarbon-impacted sites have shown high soil conductivity coincident with zones of hydrocarbon impact (Atekwana et al., 2000; Werkema, 2002). In the study area, in-situ high resolution (~5-cm interval) soil conductivity measurements showed distinct zonations coincident with the different phases of hydrocarbon impact. Higher bulk soil conductivity occurred in zones with free product and/or residual phase contamination compared to background (Werkema, 2002). Recently, Sauck et al., (1998), Atekwana et al., (2000), and Sauck, (2000) have proposed a conceptual model which attributes the high soil conductivity in hydrocarbon contaminated soils to microbial degradation of hydrocarbons and subsequent reaction of the by-products (carbonic and organic acids) with the aquifer minerals. The secondary reactions from organic and carbonic acids and the aquifer minerals increase the total dissolved solids (TDS) and thus the electrical conductivity

of the impacted soil and groundwater.

Microbial studies of soil cores and groundwater from the study area have reported the presence of hydrocarbon-degrading microorganisms (Cassidy et al., 2002; Duris et al., 2000). Volatile organic acids and biosurfactants in groundwater contaminated with hydrocarbons relative to uncontaminated groundwater provide additional evidence of intrinsic biodegradation of hydrocarbons at this site (Cassidy et al. 2002).

In this study, we have taken advantage of conductivity zonations documented by high resolution vertical soil conductivity profiling to guide our groundwater sampling. Our purpose was two fold: (1) to provide geochemical evidence for biodegradation to determine if high soil conductivity is due to biomineralization of hydrocarbon, and (2) to investigate redox processes within the aquifer. Geochemical data from closely spaced sampling allows for a better understanding of the link between geochemical changes related to microbial hydrocarbon biodegradation, and changes in the bulk conductivity signature.

Study Site

This study was conducted in a shallow hydrocarbon-contaminated aquifer at a former refinery (Crystal Refinery) located in Carson City, Michigan, USA (Fig. 1). Detailed descriptions of the study site can be found in Atekwana et al., (2000) and Werkema et al., (2000). Hydrocarbon released from storage facilities and pipelines more than 50 years ago impacted soil and groundwater at this site (Dell Engineering,

1992). Within the contaminated portion of the aquifer, different phases of hydrocarbon impact are recognized, namely, zones where residual and dissolved phase hydrocarbons (RDH) occur and zones where these phases coexist with free product (RDFH). The aquifer at the study area is approximately 4.6 to 6.1 m thick and is composed of glacial sediments consisting mostly of fine to medium sands, coarsening with depth to gravel below the water table. The aquifer is predominantly quartz with minor amounts of calcite, albite, anorthite, gypsum, and dolomite. Depth to the water table varies from 0.6 m to 0.9 m west to 4.6 to 5.8 m in the eastern portion of the study area. Water table levels vary up to 90 cm annually at the site (Atekwana et al. 2000; Werkema et al. 2000). Within the study area groundwater elevation data from June 2000 indicate groundwater flow to the west and southwest (Fig. 1). This confirms previously studies indicating groundwater flow is towards a nearby creek (Dell Engineering, 1992). Groundwater velocity of 1.68 m/day under a hydraulic gradient of 0.0015 was calculated for the site using a large network of groundwater monitoring wells (Dell Engineering, 1992).

Methods

Site Instrumentation

The study site has been instrumented at several locations with vertical resistivity probes (VRP's) for measuring soil conductivity, a water table monitoring well, and multilevel piezometers (MLP's). Werkema et al., (2000) and Werkema (2002) provide details of the VRP installation and soil conductivity measurements.

Monitoring wells and MLPs were installed using a Geoprobe® drill rig. Water table monitoring wells were constructed of 2.54-cm PVC casing fitted with 152 cm slotted PVC screens and screened across the water table. MLPs were constructed of 6.4 mm PVC tubing fitted with a 15 cm screen. MLP screened intervals were spaced at approximately 30 cm. The bundled MLPs were installed from the base of the aquifer into the vadose zone to accommodate seasonal fluctuations in the water table. The locations of the MLPs are shown in Fig. 2. Previous studies (Atekwana et al., 2000; Werkema et al., 2000) have shown that MLP-9 is located in an uncontaminated portion of the aquifer, MLP-3 and MLP-10 are located in portions of the aquifer contaminated with RDH, and MLP-1, MLP-5, and MLP-8 are located in portions of the aquifer contaminated with RDFH (Fig. 2).

Sampling and Analyses

Water from each MLP was pumped to the surface using a peristaltic pump. The water was passed through a flow cell into which a HydroLab™ downhole Minisonde was immersed. Water temperature, pH, and specific conductance (SpC) were monitored and recorded after stabilization. Alkalinity as bicarbonate was measured in the field by potentiometric titration using 1.5N H_2SO_4 to an acid equivalent point of 4.5 (Hach, 1992). Samples for analysis for benzene, toluene, ethyl benzene, and xylenes (BTEX) were collected without headspace in pre-acidified 40 ml glass vials fitted with teflon-lined screw caps, stored on ice, and transported to a commercial laboratory for analysis using EPA Method 2020. Total petroleum

hydrocarbon (TPH) was determined by summation of the BTEX compounds. Water for chemical analyses for NO_3, SO_4, Cl, NH_4, Fe, and Mn was collected in 250 ml polyethylene bottles, stored on ice, and transported to a commercial laboratory for analysis. Analyses for NO_3, SO_4, Cl and NH_4 were conducted using a Dionex DX500™ ion chromatograph (Dionex Corp., Sunnyvale, CA) equipped with a conductivity detector and an AS40 auto sampler. Total Fe and Mn were measured using a Leeman Labs P950 Inductively Coupled Plasma-Atomic Emission Spectrometer (ICP-AES) equipped with a CETAC Corp. AT5000+ ultrasonic nebulizer.

Water for DIC and carbon isotopic analysis was collected and analyzed using a modified gas evolution extraction technique (Atekwana and Krishnamurthy, 1998). DIC concentrations are reported in mg C/l. Weathered oil samples for carbon isotope analysis were collected from zones containing free product in MLP-5. Samples were oxidized with CuO in a sealed quartz tube at 900°C for 3 hours. CO_2 was purified on a vacuum line and analyzed for carbon isotope ratio. Isotope measurements were made using a Micromass Isotope Ratio Mass Spectrometer at Western Michigan University, Kalamazoo, MI, USA and are reported in the δ notation where:

$$\delta^{13}C\ (‰) = ((R_{sample} / R_{standard}) - 1) \times 10^3$$

R is $^{13}C/^{12}C$. $\delta^{13}C$ values are reported relative to VPDB. Routine $\delta^{13}C$ measurements have an overall precision of better than 0.1‰.

Results

Sample details, the results of bulk soil conductivity, and geochemical and isotopic data are shown in Table 1. All of the data presented was obtained from the saturated zone. Bulk soil conductivity was initially recorded as resistivity. In this study, the resistivity is presented as its reciprocal, the bulk conductivity, in milliSiemens per meter (mS/m). The bulk soil conductivity represented is the average of conductivity readings from within the screened interval. The "excess" CO_2 is the difference between the DIC and alkalinity in similar units (mg C/l) expressed as a percent of the alkalinity (Nascimento et al., 1997). Log pCO_2 in atmospheres (atm.) was calculated from geochemical speciation modeling using PHREEQC incorporated in the geochemical software program AQUACHEM (Waterloo Hydrogeologic, Inc., 1997).

To facilitate comparison of the bulk soil conductivity and chemical data, depth profiles of bulk soil conductivity are plotted alongside vertical profiles of chemical and isotopic parameters measured for each MLPs (Figs. 2 to 4).

Bulk Soil Conductivity

In the uncontaminated (background) portion of the aquifer (MLP-9), the bulk soil conductivity was ~3.5 mS/m at the top of the aquifer and increased to a maximum of 18 mS/m at 224.5 m (Fig. 2a). Below this elevation the bulk soil conductivity remained nearly constant at 16 mS/m to the base of the aquifer. Lower conductivities were also observed at top of the aquifer for RDH and RDFH locations

(Figs. 2b-f). However, a pronounced bulk conductivity increase was observed in deeper portions of the aquifer at contaminated locations in comparison to the background location. Bulk conductivity ranged from 10 to 25 mS/m at the RDH locations (MLP-3 and MLP-10, Figs 2b-c). Bulk conductivities were between 12 to 32 mS/m at the RDFH locations (MLP-1, 5, and 8; Figs. 2d-f). Generally, steep bulk conductivity gradients, at the centimeter scale, occur in the vertical profiles for all locations. The magnitude of the conductivity was lower in background compared to contaminated locations and there was variability in the magnitude with depth at contaminated locations.

Total Petroleum Hydrocarbon (TPH)

The highest TPH values were measured at MLP-5 and 8 (481 and 34 mg/l, respectively) (Table 1). TPH generally decreased with depth with maximum concentrations often occurring at depth intervals coincident with maximum bulk soil conductivity (Figs. 2h-l). Maximum TPH in groundwater from RDH locations was 15 mg/l (MLP-3) and 8 mg/l (MLP-10), with decreasing or non-detectable concentration within the deepest parts of the aquifer (Figs. 2h-i). Highest TPH were reported in locations with RDFH (Figs. 2j-l).

Distribution of Water Quality Parameters

Except for MLP-10, temperature was generally higher at contaminated locations (12.0 to 19.1°C) compared to background (11.7 to 13.7°C) (Table 1). pH

was generally higher (>7) at the uncontaminated location (Fig. 3m) compared to the contaminated locations (Fig. 3n-r). At the contaminated locations the pH was < 7 but generally increased towards the base of the aquifer. The specific conductance (SpC) was generally lower at the top of the aquifer and increased with depth at both contaminated and contaminated locations (Table 1). On the average, SpC was higher at contaminated locations reaching maximum values of 1112 µS at MLP-10 compared to a maximum value of 875 µS at the background location (MLP-9). Chloride was lowest at the top of the aquifer and generally increased towards the base of the aquifer at both contaminated and background locations (Table 1).

Distribution of Redox Sensitive Species, Alkalinity, DIC and $\delta^{13}C_{DIC}$

Nitrate was measurable in groundwater for all depths at the background location (MLP-9) (Fig. 2m). However, NO_3 was generally at low to non-detectable levels at locations with RDH (MLP-10, Fig. 2i) and RDFH (MLP-1 and MLP-8, Figs. 2p and 2r). At MLP-3 elevated NO_3 was measured at the base of the aquifer (Fig. 2n) and at MLP-5 and 8 (Figs. 2q-r) NO_3 was measured at top of the aquifer. Generally where NO_3 was present, NH_4 was low or absent and vice versa. Hence, all contaminated locations show high NH_4 (Figs. 2t-x) with maximum values observed at MLP-3 and 10 with RDH (Figs. 2t-u).

Total dissolved Mn was generally low within the aquifer reaching 161 µg/l at the background location (MLP-9, Fig. 3g). Overall, locations with RDH had higher Mn (Figs. 3h-i). The highest concentration (1,466 µg/l) occurred at MLP-3 (Fig 3h).

Total dissolved Fe was low in groundwater from the uncontaminated location and did not exceed 20 µg/l (Fig. 3m). Fe was higher in the middle and upper portions of the aquifer and lowest at the base of the aquifer (Figs. 3n-r) and exceeded 23,000 µg/l in groundwater from MLP-10 (Figs. 3o). At MLP-3 and 10, maximum Fe occurred at depths coincident with maximum TPH and zones of maximum bulk soil conductivity (Figs. 2h-i; and Figs. 3n-o).

Sulfate at the background location ranged from 19 to 45 mg/l and increased at depth to the base of the aquifer (Fig. 3s). At MLP-3, SO_4 ranged from 24 to 47 mg/l near the water table to non-detectable at the middle of the aquifer, increasing to about 83 mg/l at the base of the aquifer at (Fig. 3t). At MLP-10, SO_4 was about 3 mg/l at the water table, but decreased to non-detectable levels in the middle portion of the aquifer, and increased to 80 mg/l at the base of the aquifer (Fig. 3u). At locations with RDFH (e.g. MLP-1 and 5, Figs. 3v-w), SO_4 was non-detectable at most depths, however, at MLP-8, low concentrations at the water table increased steadily to about 85 mg/l at the base of the aquifer (Fig. 3x).

Generally, alkalinity was lower at top of the aquifer and increased with depth (Fig. 4g-l). Alkalinity was also lower at the background location (MLP-9) reaching a maximum of 320 mg/l (Fig. 4g). Overall, alkalinity was higher at RDH locations (MLP-3 and 10, Figs. 4h-i), and reached a maximum of 547 mg/l at MLP-3. DIC showed a similar trend to alkalinity. DIC was lower (< 100 mg C/l) at the background location (Fig. 4m) and higher at contaminated locations, reaching a maximum of 206 mg C/l at MLP-3 (Fig. 4n). The $\delta^{13}C_{DIC}$ for groundwater at the

uncontaminated location ranged from –14.6 to –12.3‰ and decreased slightly with depth (Fig. 4s). At the contaminated locations the $\delta^{13}C_{DIC}$ was more negative at the top of the aquifer (–24.2 to –16.9‰) and generally more positive at depth (Figs. 4t-x). In general, more negative $\delta^{13}C_{DIC}$ values in the range of –11.3 to –16.8‰ were observed below the water table at MLP-3 and 10, the RDH locations (Figs. 4t-u). More positive $\delta^{13}C_{DIC}$ values were observed in groundwater at locations with RDFH where values reached +6.5‰ (MLP-5, Fig. 4w).

Discussion

Geochemical data for this study was acquired in late spring during seasonal recharge to the aquifer. Generally low chloride concentrations occur at the top of the aquifer. This distribution may reflect groundwater dilution due to local recharge. Depth profiles of bulk soil conductivity and profiles for redox sensitive parameters, DIC, and $\delta^{13}C_{DIC}$ from groundwater show steep vertical gradients. The steep geochemical and isotopic gradients are examined within the context of microbial mineralization of hydrocarbons at the site.

Background Location

The groundwater chemistry at MLP-9 represents geochemical conditions in the uncontaminated portions of the aquifer. Here the maximum bulk soil conductivity was <18 mS/m and was coincident with maximum alkalinity and DIC (Figs. 4m and s). Thus, assuming uniform porosity, the bulk soil conductivity at MLP-9 reflects the

pore fluid chemistry that is due largely to groundwater evolution under natural conditions. Further, Cassidy et al (2002) reported that low biosurfactant production and high surface tension (72 dynes/cm) are associated with uncontaminated groundwater at the site. The $\delta^{13}C_{DIC}$ values (–12 to –14‰) suggests that normal groundwater evolution is dominated by the dissolution of carbonate in equilibrium with soil CO_2 derived from a carbon source with $\delta^{13}C_{DIC}$ close to –27‰ (Clark and Fritz, 1997).

Locations With Dissolved and Residual Phase Hydrocarbons (RDH)

The depth profiles for MLP-3 and MLP-10 show broad overlap of zones with high bulk soil conductivities with those exhibiting depletion of TEAs (e.g. NO_3 and SO_4, Figs. 2b-c, n-o, and 3t-u) and those showing increases in metabolic by-products resulting from the reduction of NO_3, Mn(IV), and Fe(III) (Figs. 2t-u, 3h-i, 3n-o). Furthermore, the bulk conductivity and alkalinity, DIC, and $\delta^{13}C_{DIC}$ profiles also show broad overlap (Figs. 4b-c, h-i, n-o, t-u). Steep geochemical and carbon isotopic gradients accompany the chemical shifts evident in the vertical profiles for MLP-3 and 10 (Figs. 2, 3 and 4 (h-i, n-o, t-u)). The chemical shifts are most notable when ionic species such as NH_4, Fe(II), and Mn(II) succeed their electron acceptor precursors. For example, at MLP-3 increases in NH_4 from 2.5 to 29.7 mg/l, Fe(II) and Mn(II) from 4,222 to 11,904 µg/l and from 333 to 1,013 µg/l, respectively, were observed over a 50 cm interval (224.2 to 224.7 m) and provide strong evidence for chemical inhomogeneity within this interval. At MLP-10 increases in NH_4 (from 4 to

>20 mg/l), Fe(II) (from 7,326 to 23,124 µg/l), and Mn(II) (from 531 to 1,231 µg/l) within a <1m interval also confirm the chemical inhomogeneity related to the reduction of TEAs.

At MLP-3 and 10 the intervals with high TPH show depletion of NO_3 and elevated NH_4, Mn(II), and Fe(II), the metabolic by products from the reduction of NO_3, Mn(IV) and Fe(III) within the aquifer. Apparently the zones of high TPH in MLP-3 and 10 (Figs. 2h-i) provide available substrate for enhanced microbial activity. The intervals with depleted NO_3 have elevated NH_4 (Figs. 2n-o, t-u). Where increases in NO_3 occur (e.g. at the base of the aquifer in MLP-3, Fig. 2n) there is no NH_4. Assuming no other contributory sources of NH_4 exist adjacent to the site, the NO_3–NH_4 relationship suggests that dissimilatory NO_3 reduction is occurring (Bulger et al., 1989; Smith et al., 1991b; Cozzarelli et al., 1999). Higher dissolved Fe(II) and Mn(II) within the contaminated intervals indicate that both Fe(II) and Mn(II) are being released to the aquifer most likely through the reduction of Fe(III) and Mn(IV) that coat the mineral grains of the aquifer matrix (Jensen et al., 1998; Tuccillo et al., 1998; Kennedy et al., 1999).

It is inferred from the high SO_4 that occur at or close to the top of the aquifer at MLP-3 that SO_4 is being supplied during recharge. Variability in SO_4 in the vertical profiles for MLP3 and 10 is also evident as certain zones within the aquifer show relative enhancement and depletion of SO_4 (Figs. 3t-u). The SO_4-depleted zones are likely due to microbial utilization of SO_4 during hydrocarbon degradation. Based on the distribution of NO_3 and SO_4, and the influx of NH_4, Mn(II), and Fe(II)

from the reduction of NO_3, Mn(IV) and Fe(III) in the vertical profiles it appears that the reduction of NO_3, Mn(IV), Fe(III), and SO_4 are important redox reactions occurring in the aquifer at these locations. At MLP-3 high NO_3 and SO_4 occur at the base of the aquifer (Figs. 2n and 3s) together with low TPH (Fig. 2h), which suggests that substrate availability is an important limiting factor in microbial hydrocarbon degradation.

The DIC and $\delta^{13}C_{DIC}$ provide further evidence of microbial hydrocarbon degradation in groundwater at MLP-3 and 10. It appears that the groundwater in these MLPs have evolved under similar geochemical conditions as indicated by the DIC and $\delta^{13}C_{DIC}$ data. At these MLPs, groundwater at the top of the saturated zone had low DIC and depleted $\delta^{13}C_{DIC}$ (–24.2 and –22.2‰, respectively) (Figs. 3n-o, t-u). The low DIC is attributed to the presence of recharge water. The presence of RDH at MLP-3 and 10 suggests that the $\delta^{13}C_{DIC}$ was influenced by microbial degradation of hydrocarbons at the top of the saturated zone. At MLP-3 and 10, groundwater below the top of the saturated zone exhibits high DIC and the $\delta^{13}C_{DIC}$ ranges from –16.8 to –13.3‰ in MLP-3, and from –15.7 to –11.3‰ in MLP-10 (Figs. 3t-u). The high DIC is due to increased CO_2 production associated with microbial degradation of hydrocarbons. The range of $\delta^{13}C_{DIC}$ is similar to that for background groundwater and is within the range for groundwater evolving by carbonate reaction with soil CO_2 in southwest Michigan (Nascimento et al., 1997). Within the range of $\delta^{13}C_{DIC}$ values reported for groundwater below the top of the saturated zone at MLP-3 and 10, the more positive $\delta^{13}C_{DIC}$ values are observed where reduction of NO_3, Mn(IV), Fe(III),

and SO_4 is occurring. These redox reactions apparently proceed under conditions where isotopic exchange dominates because isotopic fractionation related to kinetic isotope effects generally result in much larger shifts in the $\delta^{13}C_{DIC}$ signature.

The vertical variation in the calculated pCO_2 and "excess" CO_2 for MLP-3 and MLP-10 (Table 1) also provide supporting geochemical evidence for microbial hydrocarbon degradation at these locations. Intervals with high pCO_2 overlap with intervals that show low pH, high TPH, alkalinity, and DIC. This suggests that microbial degradation of hydrocarbons produces CO_2 that results in the lowering of the pH, which induces carbonate dissolution and increases the alkalinity (Stumm and Morgan, 1995). This is not surprising because redox reactions contribute CO_2 and bicarbonate to the groundwater in excess of background (Herczeg et al., 1991; Bennett et al., 1993).

Observations of the interrelationships between bulk soil conductivity, TPH, NO_3, Mn(IV), Fe(III), and SO_4 reduction, the distribution of NH_4, Mn(II), and Fe(II), and the production of CO_2, alkalinity and DIC are significant because they not only provide a qualitative assessment of the various redox processes operative in the aquifer but they also suggest that that redox zones within the contaminant plume are reflected in the bulk conductivity signature.

Locations With Dissolved, Residual and Free Phase Hydrocarbons (RDFH)

At MLP-1, 5 and 8 the groundwater chemistry data showed that intervals where depletion of NO_3 and SO_4 occurred were coincident with decreased TPH (Figs.

2d-f, j-l, and Figs. 3v-x) and increased NH_4 and dissolved Mn(II) and Fe(II) (Figs. 2v-x, and Figs. 3j-l, p-r). Elevated NO_3 at the top of the aquifer in MLP-5 and 8 (Figs. 2q-r) probably reflects contributions to the aquifer by infiltrating water. Generally, NO_3 depletion throughout most of the aquifer at these locations is accompanied by higher NH_4 (Figs. 2v-x). The NO_3–NH_4 relation-ship is consistent with observations at MLP-3 and MLP-10 suggesting that increased NH_4 in the presence of low to non-detectable concentrations of dissolved NO_3 results from dissimilatory NO_3 reduction. The distribution of total dissolved Fe(II) and Mn(II) is consistent with the reduction of Fe (III) and Mn(IV).

Sulfate is relatively low or non-detectable in the vertical profiles of MLP-1 and MLP-5 (Figs. 3v-w) indicating that SO_4 reduction is an important redox process in groundwater at these locations. However, higher SO_4 observed in MLP-8 (Fig. 3x) probably reflects contributions to the aquifer from infiltrating water. At MLP-8, a zone of low to non-detectable SO_4 occurs at and close to the top of the water table. Below this zone SO_4 increased gradually towards the base of the aquifer. The increase in SO_4 occurred within a zone of low TPH (Figs. 2l and 3x), which suggests that the lack of available carbon substrate may inhibit the progress of SO_4 reduction at this location.

Alkalinity and DIC profiles are similar for MLP-1, 5, and 8 (Figs. 4p-r, v-x). The similarity of the profiles indicates that these parameters are interrelated because microbial hydrocarbon degradation generates CO_2 that contributes to the alkalinity and DIC. The vertical profiles of $\delta^{13}C_{DIC}$ for MLP-1, 5, and 8 showed changes in the

isotopic ratio from the top of the water table to the base of the aquifer. The magnitude of the change in the $\delta^{13}C_{DIC}$ ratio provides an insight into the geochemical processes operative within the aquifer. At MLP-1, 5 and 8 negative $\delta^{13}C_{DIC}$ values (–16.9‰, –24. 2‰ and –22.2‰, respectively), occur at the top of the saturated zone. These negative $\delta^{13}C_{DIC}$ values are probably due to microbial degradation of hydrocarbons at the top of the water table. Recent studies (Werkema et al., 2000) indicate that the water table-capillary fringe in the contaminated portions of the aquifer is marked by large numbers of oil-degrading bacteria. Because redox reactions convert the isotopically light hydrocarbons to CO_2 with little or no fractionation, it is expected that DIC added to the system would have a $\delta^{13}C_{DIC}$ signature close to the measured $\delta^{13}C$ of the hydrocarbons at the location, which vary between –26 to –28‰.

Although such an interpretation is consistent with the data for MLP-5 and 8, the negative $\delta^{13}C_{DIC}$ values may also reflect contributions from CO_2 respired from local vegetation at the site ($\delta^{13}C$ ~–26 to –28‰) (Nascimento et al., 1997). However, in MLP-1, the observed $\delta^{13}C_{DIC}$ (–16.9‰) is relatively heavy if microbial degradation of the hydrocarbons or organic matter oxidation is the sole source of CO_2. This suggests that the observed $\delta^{13}C_{DIC}$ value may be due to isotopic exchange between CO_2 derived from hydrocarbon degradation near the top of the aquifer and dissolved carbonate.

Below the water table, the $\delta^{13}C_{DIC}$ for MLP-1 and 5 document methanogenic conditions in aquifer. The $\delta^{13}C_{DIC}$ values are more positive ranging from +1.8 to –

1.9‰ in MLP-1 to +6.5 to –4.4‰ in MLP-5 (Table 1). Such high $\delta^{13}C_{DIC}$ values in groundwater are indicative of methanogenesis (e.g. Grossman et al., 1989; Herczeg et al., 1991; Conrad et al., 1997; Chapelle et al., 1998). The $\delta^{13}C$ of CH_4 in soil gas samples collected at these locations in November 1999 ranged from –26.4 to –37.7‰ (E. Atekwana, unpublished data). Microbial degradation of petroleum hydrocarbons under methanogenic conditions produces ^{13}C-depleted CH_4 (Whiticar et al., 1986).

At MLP-8 the $\delta^{13}C$ values are more negative below the water table (–9.5 to –13.5‰) compared to MLP-1 and 5, and in spite of the presence of free phase hydrocarbons at MLP-8, there is no evidence for methane production in groundwater at this location. Apparently, methanogenesis is inhibited by the presence of SO_4 because sulfate-reducing bacteria can out compete methanotrophs for available substrate (Chapelle et al., 1995). Additionally, at this location multiple bulk soil conductivity peaks occur between 224.5 to 225 m that may be related to the presence of free product at the top of the saturated zone. Below 224.5 m the increase in bulk soil conductivity (Fig.5d) is coincident with higher $\delta^{13}C_{DIC}$ values (–9.5 to –10‰) (Fig. 5v). This suggests a link between ongoing geochemical processes, which is recorded by the isotopic signature and the bulk soil conductivity measurements.

Sources of DIC

The DIC and the $\delta^{13}C_{DIC}$ have been used to infer microbial degradation of hydrocarbons (Aggarwal and Hinchee, 1991; Van Velde et al., 1995; Landmeyer et al., 1996; Conrad et al., 1997; Bolliger et al., 1999; Hunkeler et al., 1999). In

assessing microbial contributions to the groundwater DIC it is important to resolve groundwater DIC into its component species. The measured DIC represents the total inorganic carbon (CO_2, HCO_3^-, and CO_3^{2-}) whereas the major contributors to alkalinity are HCO_3^- and CO_3^{2-}. The difference between the DIC and alkalinity is "excess CO_2" that can be used as evidence for additional input into the groundwater DIC pool (Nascimento et al., 1997). Hence measurements of the DIC, alkalinity, and the $\delta^{13}C_{DIC}$ in groundwater from uncontaminated and contaminated portions of the aquifer zone are required to successfully evaluate the contribution of inorganic carbon from hydrocarbon degradation (Chapelle and Knobel, 1986).

In the study area the pH range for the groundwater samples suggest that the contribution from CO_3^{2-} is negligible, therefore, most of the alkalinity is present as HCO_3^-. In southwest Michigan, the $\delta^{13}C$ values of DIC in carbonate-rich groundwater from aquifers in glacially derived sediments is controlled by the native carbonate minerals and the $\delta^{13}C$ of soil CO_2. A value of +1.5‰ is assumed for the $\delta^{13}C$ of soil carbonates (Nascimento et al., 1997) and an average $\delta^{13}C$ of –27‰ is assumed for the vegetation, which is dominated by C-3 plants typical of temperate humid environments. Diffusion of soil CO_2 from the vadose zone is expected to modify the $\delta^{13}C$ of soil CO_2 (Cerling, 1984). Assuming the soil CO_2 is derived solely from the soil carbon in the uncontaminated parts of the site, the $\delta^{13}C$ of soil CO_2 is expected to be around –23‰. Dissolution of soil CO_2 by infiltrating recharge leads to hydration and eventual dissociation into HCO_3^- and CO_3^{2-} and the fractionation associated with this process yields groundwater with a $\delta^{13}C_{DIC}$ around –15‰ at 10°C

and DIC around 65 mg C/l (Nascimento et al., 1997).

DIC and $\delta^{13}C_{DIC}$ and Groundwater Evolution

The $\delta^{13}C_{DIC}$ values were plotted against DIC (Fig. 5). Also plotted on Figure 5 is the DIC and $\delta^{13}C_{DIC}$ composition of uncontaminated southwest Michigan groundwater (Nascimento et al., 1997). Three distinct groundwater groupings can be identified consisting of: (1) water from the top of the aquifer in the contaminated portions of the aquifer characterized by low DIC (<55 mg C/l) and $\delta^{13}C_{DIC}$ ranging from –24.2 to –22.2‰ (Group I), and includes groundwater from MLP-3, 5, 8 and 10; (2) groundwater from both uncontaminated and contaminated portions of the aquifer (Group II). Uncontaminated groundwater has low DIC (30 to 87 mg C/l) and $\delta^{13}C$ ranging from –12 to –14‰. Contaminated groundwater has higher DIC (64-206 mg C/l) and $\delta^{13}C$ ranging from –16.9 to –9.5‰, among these are groundwater samples from MLP- 8, a location that contains free product; and (3) groundwater from contaminated wells (MLP-1 and 5) containing free product with DIC ranging from 90 to 165 mg C/l and $\delta^{13}C$ ranging from –4.4 to +6.5‰ (Group III).

The low $\delta^{13}C_{DIC}$ (–24 to –22‰) for samples collected from the top of the aquifer in the contaminated portions of the aquifer (Group I) indicate a CO_2 source for the DIC that is generated from microbial degradation of hydrocarbons at the top of the water table. The low DIC is consistent with a short residence time for recharge water in the aquifer hence little opportunity is available to enhance DIC concentration through mineral dissolution. Furthermore, low DIC in the presence of relatively high

"excess" CO_2 observed in the groundwater provides evidence for the presence of CO_2 gaseous phase within this zone. It is plausible that for groundwater within this group $\delta^{13}C_{DIC}$ evolution to more positive values could occur by dissolution of carbonate (+1.5‰) present in the aquifer.

The DIC and $\delta^{13}C_{DIC}$ in groundwater from Group II are influenced by a range of microbial processes including aerobic respiration at background locations, and redox processes such as the reduction of NO_3, Mn(IV), Fe(III), and SO_4 at contaminated locations. Background groundwater from the study area has DIC and $\delta^{13}C_{DIC}$ values close to that for uncontaminated groundwater from southwest Michigan. Within the contaminated zones, the increase in CO_2 due to microbial hydrocarbon degradation increases the DIC, hence, the groundwater DIC evolves along a path parallel to the x-axis (Fig. 6). Furthermore, the groundwater isotopic evolution is controlled by the dissolution of carbonate resulting from enhanced CO_2 production, and the range of $\delta^{13}C_{DIC}$ values (between –16 to –9‰) are consistent with this observation.

Groundwater $\delta^{13}C_{DIC}$ evolution to more positive values requires the establishment of methanogenic conditions in the aquifer. Groundwater DIC evolution in Group III is consistent with methanogenesis. Within this group, groundwater at MLP-5 has a larger range of DIC and $\delta^{13}C_{DIC}$ values compared to MLP-1. At MLP-5 lower DIC occur close to the top of the water table where dilution by recharge may be a factor. At depth, the $\delta^{13}C_{DIC}$ becomes more positive. At MLP-1 the range of DIC is narrow, which suggest that CO_2 is consumed during reduction to CH_4.

Summary and Conclusions

Geochemical and isotopic data from closely spaced vertical sampling along anomalous conductive soil zones in a shallow, hydrocarbon-contaminated aquifer were used to provide geochemical evidence for biodegradation, to determine whether high soil conductivities were due to biomineralization of hydrocarbons, and to investigate redox processes occurring within the anomalously conductive zones.

Based on the relationship between the distribution of TEAs, the DIC, and the $\delta^{13}C_{DIC}$, and redox processes identified in vertical profiles, groundwater evolution in the uncontaminated portion of the aquifer is dominated by aerobic respiration. The reactions that produce DIC appear to be the dissolution of carbonate minerals by carbonic acid produced from biogenic soil CO_2 and the microbial oxidation of organic matter deeper in the aquifer. Low bulk soil conductivities are associated with this zone.

Within the portions of the aquifer contaminated by RDH, the groundwater is anaerobic and spatial and vertical changes in groundwater chemistry, TEAs, and redox sensitive parameters indicate that the reduction of NO_3, Mn(IV), Fe(III), and SO_4 are important redox process occurring at these locations. Higher DIC compared to background reflects increased CO_2 due microbial hydrocarbon degradation. The $\delta^{13}C_{DIC}$ is influenced by the dissolution of carbonate resulting from enhanced CO_2 production. Higher bulk soil conductivities occur within this portion of the aquifer. In the portion of the aquifer contaminated by RDFH, the $\delta^{13}C_{DIC}$ indicate the presence

of methanogenic conditions at most locations, however, there is evidence to suggest that methanogenesis is apparently inhibited by the presence of SO_4. High DIC also reflects increased CO_2 due microbial hydrocarbon degradation and the highest bulk soil conductivities occur within this portion of the aquifer.

Thus the subsurface expression of microbial hydrocarbon mineralization is apparently recorded in the bulk soil conductivity measurements. It also appears that the bulk conductivity measurements record an integrated summary of process-driven biogeochemical changes reflected in the changing pattern of redox zonation. If the geochemical changes mapped in vertical profile are an acceptable analogue for the horizontal profile then the results of this study indicate that generally accepted models of well demarcated redox zones developed for numerous contaminated sites based on bulk groundwater samples obtained from individual wells are far too simplistic.

This study demonstrates that considerable variability exists in the vertical dimension that appears to be controlled by geological and biogeochemical conditions (e.g. aquifer heterogeneity, nutrients, and contaminant substrate) and creates microenvironments conducive to microbial activity in the aquifer. Researchers have become increasingly aware of this situation (Bekins et al., 2001; Cozzarelli et al., 2001) and more attention is currently focused on acquiring geochemical (soil and groundwater) data based on fine resolution vertical sampling.

Table 1. Bulk Conductivity of Soils, TPH, Temperature, pH, SpC, TDS, Cl, NO_3, NH_4, Total Fe(II) and Mn(II), Alkalinity, DIC, $\delta^{13}C_{DIC}$, "Excess" CO_2, and Log pCO_2 Distribution in Groundwater from Multilevel Piezometers.

Well ID	Elevation (m)	Bulk Conductivity (mS/m)	Total Petroleum Hydrocarbon (mg/l)	Temperature (°C)	pH	Specific Conductance (µS)	Cl (mg/l)	NO_3 (mg/l)	NH_4 (mg/l)	Fe (ug/l)	Mn (ug/l)	SO_4 (mg/l)	Alkalinity (mg/l)	DIC (mg C/L)	$\delta^{13}C_{DIC}$ (‰)
MLP - 9	225.00	3.6	ND	13.5	7.1	470.3	46.4	5.6	ND	20	5	18.9	90	29.9	-12.3
(Uncont.)	224.55	18.4	ND	12.4	7.3	771.9	107.5	5.8	ND	18	5	40.5	258	71.2	-14.5
	224.07	16.1	ND	11.7	7.1	851.6	51.8	2.0	ND	18	161	44.4	311	84.7	NA
	223.78	NV	ND	13.7	7.0	875.0	50.7	2.0	ND	17	42	45.4	320	87.3	-14.6
MLP - 3	225.58	10.4	0.30	16.4	6.3	255.9	0.7	0.1	47.5	1571	212	23.5	41	30.1	-24.2
(RDH)	225.13	23.6	12.22	15.3	6.4	947.5	5.7	0.8	37.5	14539	1466	46.8	431	170.6	-16.8
	224.68	25.4	14.78	14.4	6.5	1064.0	12.1	0.1	29.7	11904	1031	5.4	547	206.3	-13.3
	224.23	21.3	0.78	14.2	6.7	1030.0	24.2	ND	2.5	4222	333	ND	526	153.3	-14.7
	223.77	21.2	0.14	13.1	6.8	919.9	40.2	ND	0.0	3382	226	36.8	420	107.7	-14.7
	223.30	22.2	0.006	13.7	6.5	910.4	47.2	21.0	ND	164	79	83.3	333	86.7	-14.0
MLP - 10	225.21	11.2	0.04	12.7	5.8	131.0	4.2	ND	1.5	4596	210	3.9	38	55.1	-22.2
(RDH)	224.76	20.0	8.29	12.5	6.1	474.0	14.3	ND	21.0	23124	1231	ND	210	114.0	-11.3
	224.31	15.3	7.57	12.4	6.5	766.5	27.8	ND	22.8	13851	833	ND	401	150.5	-11.4
	223.86	14.9	1.58	12.0	6.6	1112.0	58.6	ND	3.9	7326	539	4.0	524	151.3	-15.3
	223.38	15.2	0.00	12.3	6.6	1026.0	70.1	ND	2.5	133	129	80.4	380	99.0	-15.7
MLP - 1	225.15	30.9	FP	15.1	6.4	815.0	1.5	0.2	17.6	15912	833	10.4	415	135.3	-16.9
(RDFH)	224.69	29.2	11.48	14.5	6.4	916.2	13.2	ND	11.7	10551	365	3.8	495	163.5	-1.9
	224.24	31.9	2.00	13.6	6.5	944.0	17.2	ND	12.4	7254	257	ND	510	150.4	0.7
	223.79	32.2	2.61	14.3	6.5	945.8	17.5	ND	12.9	8825	251	ND	515	154.9	0.5
	223.34	25.9	2.00	14.4	8.5	942.7	18.9	ND	14.7	8655	246	ND	503	148.8	-0.8
	222.88	25.3	2.01	13.6	6.5	957.3	14.9	ND	13.8	8683	260	ND	521	154.0	0.6
	222.43	29.6	4.50	15.5	6.6	934.6	34.7	0.2	12.0	9036	237	ND	496	139.8	1.8
	221.96	NV	3.87	14.8	6.9	996.7	37.1	ND	9.5	6751	175	3.0	459	134.5	0.0
MLP - 5	224.96	15.2	19.30	19.1	6.1	185.4	1.0	33.1	6.0	4077	328	ND	30	45.0	-24.2
(RDFH)	224.51	23.2	481.0	FP	6.4	318.0	0.5	0.1	7.6	9639	601	1.6	206	89.9	-1.3
	224.06	18.2	3.61	15.9	6.4	931.2	17.5	1.1	4.4	8539	145	ND	509	165.4	6.5
	223.61	17.7	0.92	17.1	6.7	891.2	30.7	0.9	6.2	7298	90	ND	469	126.1	-2.3
	223.13	NV	0.76	17.0	7.1	885.4	31.0	ND	5.4	7491	97	2.0	467	130.0	-4.4
MLP - 8	224.60	12.7	33.60	FP	FP	FP	1.1	2.3	10.2	999	49	8.4	FP	27.0	-22.2
(RDFH)	224.15	17.5	5.75	13.8	6.9	577.0	15.2	0.3	5.7	6280	103	0.7	232	64.2	-10.0
	223.70	17.6	0.064	13.9	7.0	941.2	46.2	ND	5.9	6192	163	10.9	441	114.1	-9.5
	223.24	16.5	0.036	15.3	6.9	978.3	55.0	ND	2.5	3906	224	31.6	437	108.5	-11.6
	222.79	18.6	0.03	14.5	6.9	996.5	59.1	ND	1.8	3676	271	56.3	418	102.8	-12.7
	222.31	NV	0.00	15.3	7.0	985.5	62.8	ND	2.2	3832	213	85.4	379	98.0	-13.5

NA = Not Analyzed ND = Not Detected NC = Not Computed NV = No Value
FP = Free Product Uncont. = Uncontaminated Location
RDH = Locations With Residual and Dissolved Phase Hydrocarbons RDFH = Locations With Residual, Dissolved and Free Phase Hydrocarbons
Depth and Elevation Data to the top of the Screened Interval

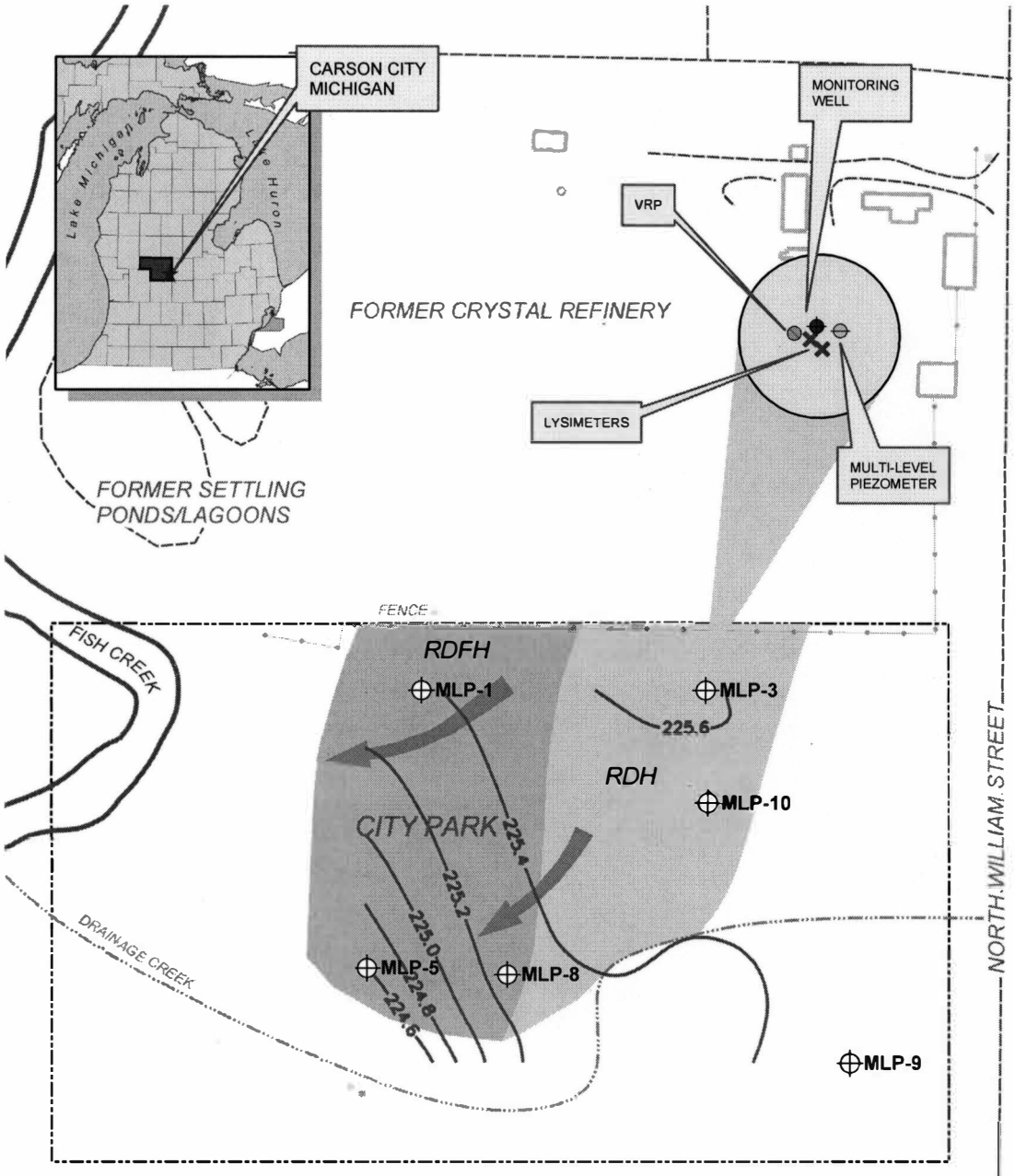

Legend

- Study Area
- Well Clusters
- Groundwater Contour
- Residual and Dissolved Phase Hydrocarbons (RDH)
- Residual, Dissolved and Free Phase Hydrocarbons (RDFH)
- Groundwater Flow Direction

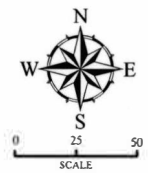

Figure 1
Study Area

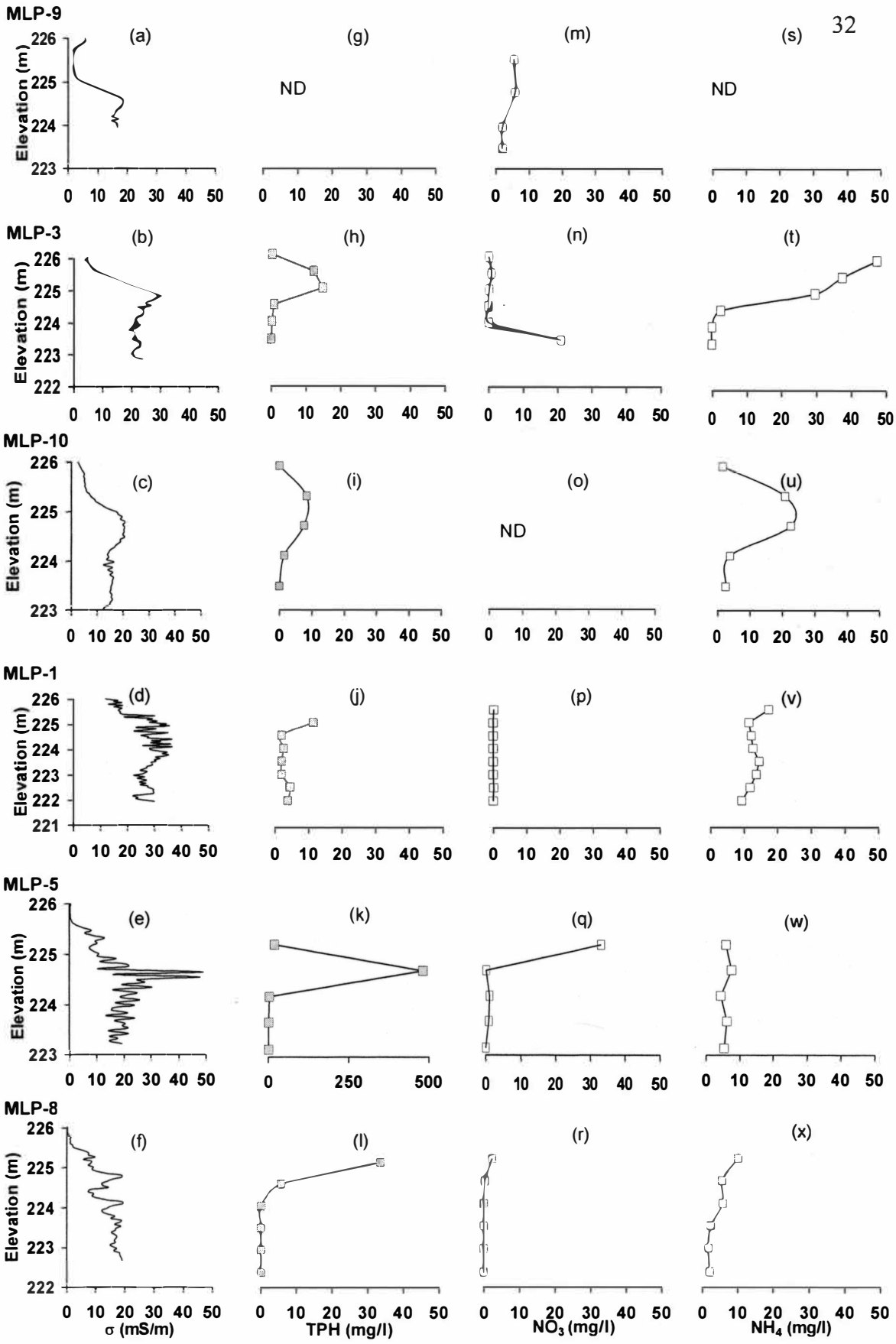

Figure 2. Vertical Profile of Bulk Conductivity of Soils, TPH, NO_3, and NH_4 in Groundwater for the Background Location (MLP-9), for Locations With Residual and Dissolved Phase Hydrocarbons (MLP-3 and MLP-10), and for Locations With Residual, Dissolved and Free Phase Hydrocarbons (MLP-1, MLP-5, and MLP-8).

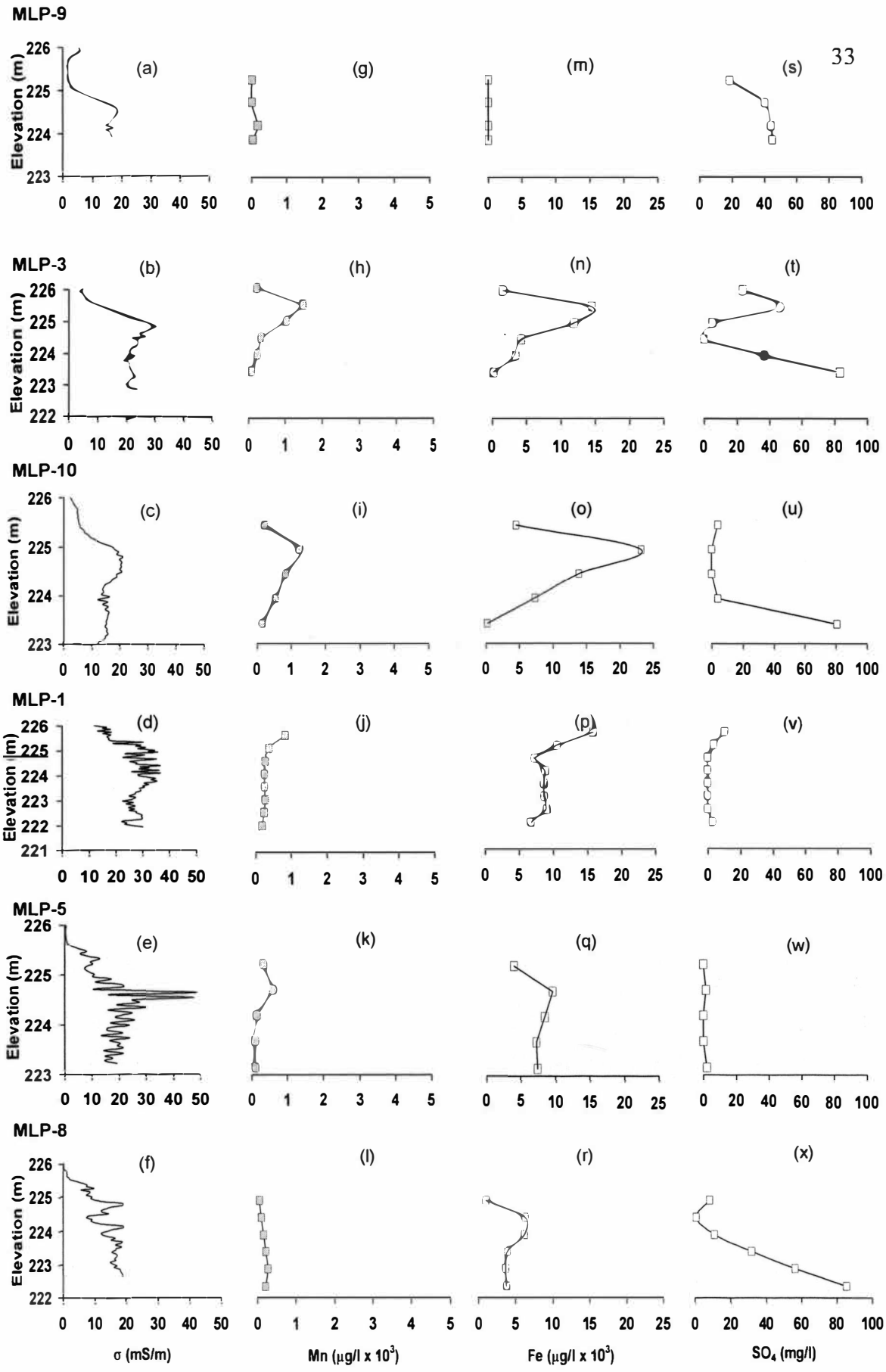

Figure 3. Vertical Profile of Bulk Conductivity of Soils, and Total Dissolved Mn(II) and Fe(II), and SO_4 in Groundwater for the Background Location (MLP-9), for Locations With Residual and Dissolved Phase Hydrocarbons (MLP-3 and MLP-10), and for Locations With Residual, Dissolved, and Free

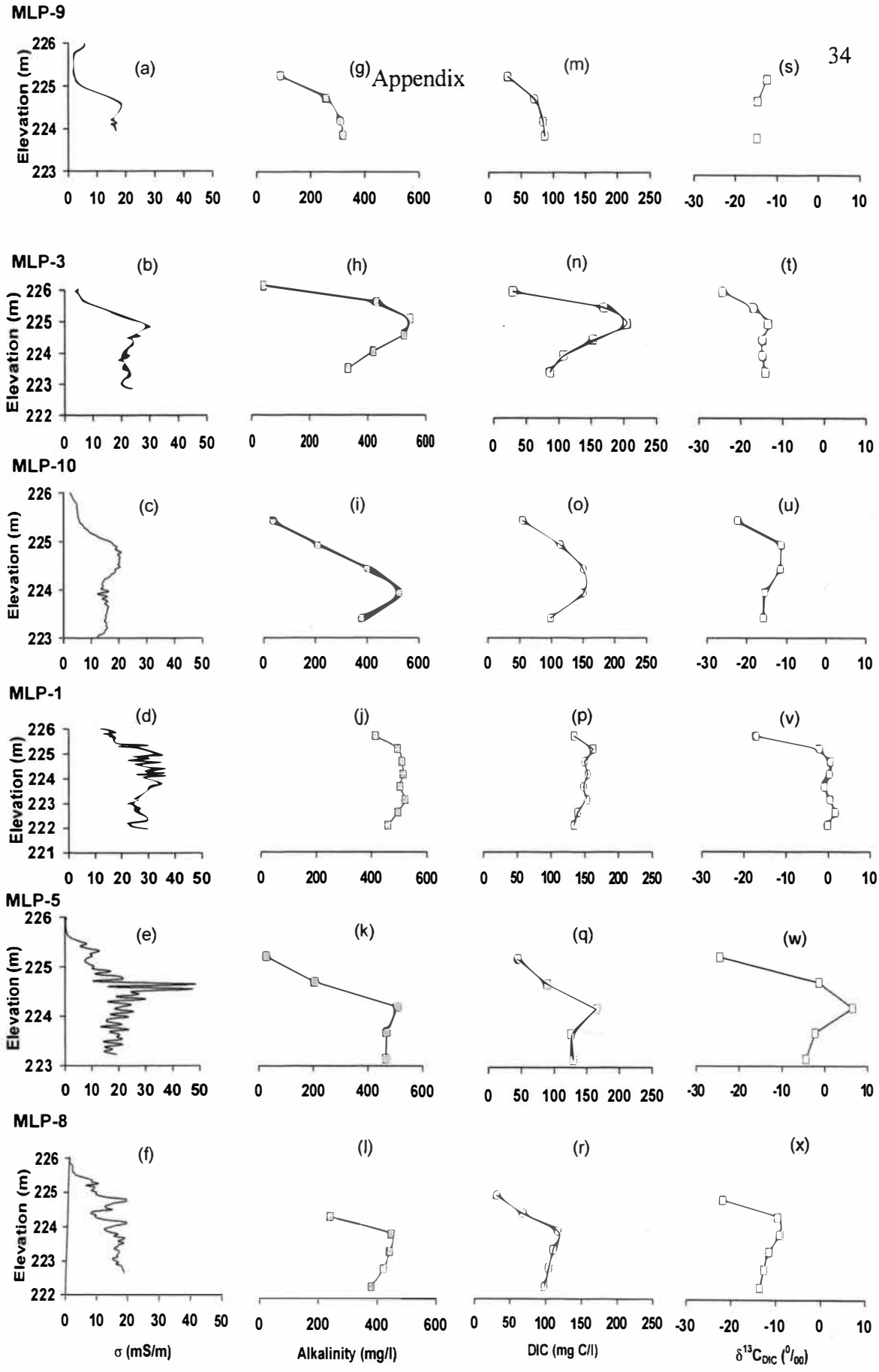

Figure 4. Vertical Profile of Bulk Conductivity of Soils, and Alkalinity, DIC, and $\delta^{13}C_{DIC}$ in Groundwater for the Background Location (MLP-9), for Locations With Residual and Dissolved Phase Hydrocarbons (MLP-3 and MLP-10), and for Locations With Residual, Dissolved, and Free Phase

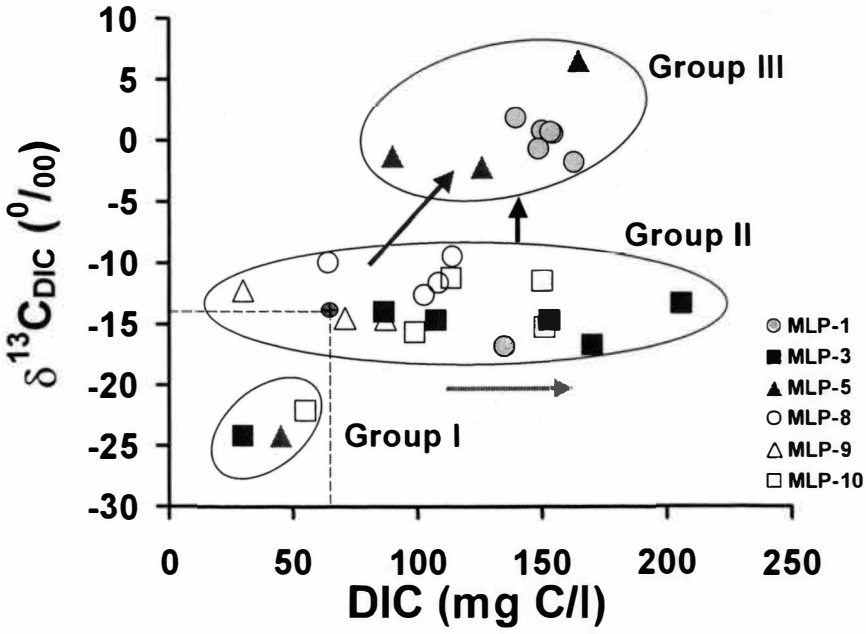

Figure 5. $\delta^{13}C_{DIC}$ Versus DIC. Arrows Show the Direction of Groundwater DIC Evolution. Representative Uncontaminated (Background) Groundwater From SW Michigan Plots Within Group II.

References

Aggarwal, P. K. and Hinchee, R. E., 1991. Monitoring in situ biodegradation of hydrocarbons by using carbon isotopes. Environ. Sci. Tech., 25: 1178-1180

Atekwana, E. A., Sauck, W. A. and Werkema, D. D., 2000. Investigations of geo-electrical signatures at a hydrocarbon contaminated site. J Appl. Geophys., 44: 167-180.

Atekwana, E. A., Sauck, W. A., Abdel Aal, G.Z. and Werkema, D. D., 2002. Geophysical investigation of vadose zone conductivity anomalies at a hydrocarbon contaminated site: Implications for the assessment of intrinsic bioremediation. (In press), J. Environ. Eng. Geophys.

Atekwana E. A. and Krishnamurthy, R. V., 1998. Seasonal variations of dissolved inorganic carbon and $\delta^{13}C$ of surface waters: Application of a modified gas evolution technique. J. Hydrol., 205: 265-278.

Bennett, P. C., Siegel, D. E., Baedecker, M. J. and Hult, M. F., 1993. Crude oil in a shallow sand and gravel aquifer - I. Hydrogeology and inorganic geochemistry. Appl. Geochem., 8: 529-549.

Bekins, B., Rittmann, B. E. and MacDonald, J. A., 2001. Natural attenuation strategy for groundwater cleanup focuses on demonstrating cause and effect. EOS, Transactions American Geophysical Union, 82(5), 53, Jan. 30, 2001.

Bollinger, C., Hohener, P., Hunkeler, D., Haberli, K. and Zeyer, J., 1999. Intrinsic bioremediation of a petroleum hydrocarbon-contaminated aquifer and assessment of mineralization based on stable carbon isotopes. Biodegradation, 10: 201-217.

Bossert, I.D. and Compeau, G.C., 1995. Cleanup of petroleum hydrocarbon contamination in soil. In: L.Y. Young and C.E. Cerniglia (Editors.), Microbial transformation and degradation of toxic organic chemicals, pp. 77-125. New York: Wiley-Liss.

Bulger, P.R., Kehew, A.E. and Nelson, R.A., 1989. Dissimilatory nitrate reduction in a waste water contaminated aquifer. Ground Water, 27: 664-671.

Cassidy, D. P., Werkema, D. D., Sauck, W. A., Atekwana, E. A., Rossbach, S. and Duris, J., 2001. The effects of LNAPL biodegradation products on electrical conductivity measurements. J. Environ. Eng. Geophys., 6: 47-52.

Cassidy, D. P, Hudak, A. J., Werkema, D. D., Atekwana, E. A., Rossbach, S., Duris, J. W., Atekwana, E. A. and Sauck, W. A., 2002. In-situ Rhamnolipid production at an abandoned petroleum refinery by *Pseudomonas aeruginosa*.(In Press), Jour. Soil and Sed. Cont.

Cerling, T. E., 1984. The stable isotopic composition of soil carbonate and its relationship to climate. Earth. Planet. Sci. Lett., 71: 229-240.

Chapelle F. H. and Knobel, L. L., 1986. Stable carbon isotopes of HCO_3^- in the Aquia aquifer, Maryland: Evidence for an isotopically heavy source of CO_2. Ground Water, 23: 592-599.

Chapelle, F.H., McMahon, P.B., Dubrovsky, N.M., Fujii, R.F., Oaksford, E.T. and Vroblesky, D.A., 1995. Deducing the distribution of terminal electron-accepting processes in hydrologically diverse groundwater systems. Water Resour. Res., 3: 359-371.

Clark, I.D. and Fritz, P., 1997. Environmental isotopes in hydrogeology. Boca Raton, FL: CRC Press.

Conrad, M. E., Daley, P. F., Fischer, M. L., Buchanan, B. B., Leighton, T. and Kashgarian, M., 1997. Combined $\delta^{14}C$ and $\delta^{13}C$ monitoring of *in-situ* biodegradation of petroleum hydrocarbons. Environ. Sci. Technol., 31: 1463-1469.

Cozzarelli, I. M., Eganhouse, R. P. and Baedecker, M. J., 1990. Transformation of monoaromatic hydrocarbons to organic acids in anoxic groundwater environment. Environ. Geol. Water Sci., 16; 135-141.

Cozzarelli, I. M., Baedecker, M. J., Eganhouse, R. P. and Goerlitz, D. F., 1994. The geochemical evolution of low-molecular-weight organic acids derived from the degradation of petroleum contaminants in groundwater. Geochim. Cosmochim. Acta., 58: 863-877.

Cozzarelli, I. M., Herman, J. S., Baedecker, M. J. and Fischer, J. M., 1999. Geochemical heterogeneity in a gasoline-contaminated aquifer. Jour. Cont. Hydrol., 40: 261-284.

Cozzarelli, I. M., Bekins, B. A., Baedecker, M. J., Aiken, G. R., Eganhouse, R. P. and Tuccillo, M. E., 2001. Progression of natural attenuation processes at a crude oil spill site: I. Geochemical evolution of the plume. Jour. Cont. Hydrol., 53: 369-385.

Dell Engineering, 1992. Remedial Action Plan for Crystal Refining Company, 801 North Williams Street, Carson City, MI. Report DEI No. 921660, Holland, MI.

Duris, J. W., Werkema, D. D., Atekwana, E. A., Eversole, R., Beuving, L. and Rossbach, S., 2000. Microbial communities and their effects on silica structure and geophysical properties in hydrocarbon impacted sediments. Geological Society of America Program with Abstracts, 32: A-190.

Grossman, E.L., Coffman, B.K., Fritz, S.J. and Wada, H., 1989. Bacterial production of methane and its influence on groundwater chemistry in east-central Texas aquifers. Geology, 17: 495-499.

Grossman, E.A., 1997. Stable carbon isotopes as indicators of microbial activities in aquifers. In: C. J. Hurst (Editor), Manual of Environmental Microbiology (pp. 565-576). Washington, DC: ASM Press.

Hach Company, 1992. Digital Titrator Model 16900-01 Manual.

Herczeg, A. L., Richardson, S. B. and Dillon, P. J., 1991. Importance of methanogenesis for organic carbon mineralization in groundwater contaminated by liquid effluent, South Australia. Appl. Geochem., 6: 533-542.

Herczeg, A. L. and Edmunds, W.M., 2000. Inorganic ions as tracers. In: P. Cook and A. L. Herczeg (Editors), Environmental tracers in subsurface hydrology (pp. 31-77). Boston: Kluwer Academic Publishers.

Hunkeler, D., Hohener, P., Bernasconi, S. and Zeyer, J., 1999. Engineered in situ bioremediation of a petroleum hydrocarbon-contaminated aquifer: Assessment of mineralization based on alkalinity, inorganic carbon and stable carbon isotope balances. Jour. Cont. Hydrol., 37: 201-223.

Jankowski, J. and Acworth, R.I., 1997. Development of a contaminant plume from a municipal landfill: Redox reactions and plume variability. In: J. Chilton (Editor.), Groundwater in the urban environment: Problems, processes and management (pp. 439-444). Proceedings of the XXVII IAH Congress on Groundwater in the Urban Environment, Nottingham, UK. Sept., 1997. A.A. Balkema Publishers.

Jensen, D. L., Boddum, J. K., Redemann, S. and Christensen, T. H., 1998. Speciation of Dissolved Iron(II) and Manganese(II) in a groundwater pollution plume. Environ. Sci. Technol., 32: 2657-2664.

Kennedy, L. G., Everett, J. W., Dewers, T., Pickins, W. and Edwards, D., 1999. Application of mineral iron and sulfide analysis to evaluate natural attenuation at fuel contaminated site. Jour. Environ. Engineering, 47-56.

Landmeyer, J.E., Vroblesky, D.A. and Chapelle, F.H., 1996. Stable carbon isotope evidence of biodegradation zonation in a shallow jet-fuel contaminated aquifer. Environ. Sci. Technol., 30: 1120-1128.

Lovely, D. R., 2000. Fe(III) and Mn(IV) reduction. In: D. R. Lovely (Editor), Environmental Microbe-Metal Interactions (pp. 3-30). Washington, DC: ASM Press.

McMahon, P. B. Vroblesky, D. A., Bradley, P. M., Chapelle, F. H. and Gullet, C. D., 1995. Evidence for enhanced mineral dissolution in organic acid-rich shallow ground water. Ground Water, 33: 207-216.

Nascimento, C., Atekwana, E.A. and Krishnamurthy, R.V., 1997. Concentrations and isotope ratios of dissolved inorganic carbon in denitrifying environments. Geophysical. Research Letters, 26(12): 1511-1514.

Rosenberg, E. and Ron, E. Z., 1996. Bioremediation of petroleum hydrocarbon contamination. In R. L. Crawford and D. L. Crawford (Editors), Bioremediation-Principles and Applications: Biotechnology Research Series, 6: pp.100-124. Cambridge, UK: Cambridge University Press.

Routh, J., Grossman, E. L., Ulrich, G. A. and Suflita, J. M., 2001. Volatile organic acids and microbial processes in the Yegua formation, east-central Texas, Applied Geochemistry, 16:183-195.

Sauck, W.A., Atekwana, E.A. and Nash, M.S., 1998. Elevated conductivities associated with an LNAPL plume imaged by integrated geophysical techniques. J. Environ. Eng. Geophys., 2-3: 203-212.

Sauck, W. A., 2000. A conceptual model for the geoelectrical response of LNAPL plumes in granular sediments. J. Appl. Geophys., 44: 151-165.

Smith, R.L, Harvey, R.W. and LeBlanc, D.R., 1991a. Importance of closely spaced vertical sampling in delineating chemical and microbial gradients in groundwater studies. Jour. Cont. Hydrol., 7: 285-300.

Smith, R.L, Harvey, R.W. and LeBlanc, D.R., 1991b. Denitrification in nitrate-contaminated groundwater: occurrence in steep vertical chemical gradients. Geochim. Cosmochim. Acta., 55: 1815-1825.

Snell Environmental Group, 1994. I. Technical Memorandum Task 1B - IRAP Evaluation, Crystal Refinery, 801 N. Williams Street, Carson City, Michigan. MERA ID #59003.

Stumm, W. and Morgan, J. J., 1995. Aquatic chemistry: Chemical equilibria and rates in natural waters, 3rd Edition. New York: John Wiley & Sons, 1022 p.

Tuccillo, M. E., Cozzarelli, I. M. and Herman, J. S., 1998. Iron reduction in the sediments of a hydrocarbon-contaminated aquifer. Applied Geochemistry, 14: 655-667.

Van de Velde, K.E., Marley, M.C., Studer, J. and Wagner, D.M., 1995. Stable carbon isotopic analysis to verify bioremediation and bioattenuation. In: R.E. Hinchee, G.S. Douglas, and S.K. Ong (Editors), Monitoring and Verification of Bioremediation (pp. 241-257). Columbus, OH: Battelle Press.

Vroblesky, D.A., and Chapelle, F.H., 1994. Temporal and spatial changes of terminal electron-accepting processes in petroleum hydrocarbon-contaminated aquifer and the significance for contaminant biodegradation. Water Resour. Res., 30: 1561-1570.

Werkema D. D., Atekwana, E. A., Sauck, W. A., Rossbach, S. and Duris, J., 2000. Vertical distribution of microbial abundances and apparent resistivity at an LNAPL spill site. Proceedings of the Symposium on the Application of Geophysics to Engineering and Environmental Problems (SAGEEP), Arlington Virginia, pp. 669-678.

Werkema D. D., 2002. Geoelectrical Response of an Aged LNAPL Plume. Implications for Monitoring Natural Attenuation. Unpublished Ph.D. Thesis, Western Michigan University, Kalamazoo, MI.

Whiticar, M.J., Faber, E. and Schoell, M., 1986. Biogenic methane formation in marine and freshwater environments: CO_2 reduction vs. acetate fermentation-Isotope evidence. Geochem. Cosmochim. Acta., 50: 693-709.

CHAPTER III

GEOCHEMICAL AND ISOTOPIC CHARACTERISTICS ASSOCIATED WITH HIGH SOIL CONDUCTIVITIES IN A SHALLOW HYDROCARBON CONTAMINATED AQUIFER: II. MINERAL WEATHERING AND HIGH SOIL CONDUCTIVITIES

Abstract

Data collected from a network of in-situ vertical resistivity probes (VRPs) deployed within a hydrocarbon contaminated aquifer showed high soil conductivities associated with zones where residual and dissolved phase hydrocarbons (RDH) occur and zones where these phases coexist with free phase hydrocarbons (RDFH). Bulk soil conductivities were highest (12 to 30 mS/m) in the RDFH zone compared to the RDH zone (10 to 25 mS/m). Groundwater from closely spaced multi-level piezometers (MLPs) installed in the aquifer was analyzed to investigate the role of mineral weathering as the source of ions responsible for the high soil conductivity. Evidence for mineral weathering in the aquifer was assessed using major inorganic ions, dissolved inorganic carbon (DIC), stable carbon isotope ratio of DIC ($\delta^{13}C_{DIC}$), and bulk soil conductivity. The link between bulk soil conductivity and $\delta^{13}C_{DIC}$ in contaminant plumes has never been reported in the literature.

The results show higher Na, Ca, and Mg in the contaminated zone compared to background. High TDS in the contaminated zones were due to elevated Na, Ca, and Mg, which is consistent with the weathering of carbonate and Na and Ca

feldspars, the dominant minerals in the aquifer. The higher TDS at the contaminated locations was also coincident with higher DIC. DIC was highest in the portion of the plume characterized by RDH. The $\delta^{13}C_{DIC}$ values of –16.9 to –9.5‰ suggest that DIC evolution within this zone is controlled by carbonate dissolution through enhanced CO_2 production related to microbial hydrocarbon degradation. Within the range of $\delta^{13}C_{DIC}$ values reported for groundwater at the RDH locations, the more positive $\delta^{13}C_{DIC}$ values were observed in zones where reduction of NO_3, Mn(IV), Fe(III), and SO_4 was occurring and was coincident with higher DIC, TDS, and bulk soil conductivity. Within the portion of the aquifer with RDFH, DIC was lower compared to the RDH location with an associated $\delta^{13}C_{DIC}$ in the range of +6.5 to –4.4‰. Both the DIC and $\delta^{13}C_{DIC}$ suggest that methanogenesis is the dominant redox process. High DIC within the methanogenic zone is also coincident with higher TDS, and bulk soil conductivity. Thus the subsurface expression of microbial hydrocarbon mineralization is recorded in the TDS, DIC, $\delta^{13}C_{DIC}$, and bulk soil conductivity. It also appears that the bulk soil conductivity records an integrated summary of process-driven biogeochemical changes reflected in the changing pattern of redox zonation. This suggests that high soil conductivities measured at hydrocarbon-contaminated sites could be used to assess the potential for natural attenuation and to monitor intrinsic bioremediation at these sites.

Introduction

Over the past decade there has been a resurgence of interest in the use of

geophysical techniques to map contaminant plumes associated with non-aqueous phase liquids (LNAPLs). Prior mapping efforts were constrained primarily by the use of geophysical models that assumed the LNAPLs to be resistive. These models did not take into account biological and geochemical changes occurring within the contaminated environment therefore they inadequately explained the geoelectrical characteristics associated with the aging of LNAPL plumes in the subsurface. Recognizing the importance of biodegradation processes on the subsurface environment, a new model presented by Sauck et al., (1998), Sauck (2000), and Atekwana et al., (2000) provides a dynamic view of hydrocarbon contaminant plumes, with their characteristics changing over time from initially resistive to conductive as the LNAPLs undergo microbial degradation (see Sauck, 2000 for a detailed explanation of this model). The conceptual model suggests that the resistivity is controlled by geologic, hydrologic and chemical factors in both background and hydrocarbon-contaminated regions of soils. Their collective work underlined the fact that successful geophysical mapping of contaminant plumes requires a multi-disciplinary approach that integrates elements of the site geology, hydrogeochemistry, and microbiology. Knight (2001) has coined the term "biogeophysics" in reference to this new approach.

In order to confirm the conductive model, first it is necessary to verify that hydrocarbon degradation is indeed occurring in the aquifer, then, proof must be garnered to demonstrate that enhanced weathering of aquifer minerals is occurring within the contaminated zone, and finally the presence of the ions resulting from

mineral weathering must be linked to the anomalous conductivity signatures. Following this approach, in this study we used data collected from a network of vertical resistivity probes (VRPs) deployed at the site (Werkema, 2002) to guide the placement of a series of MLPs within the anomalously conductive zones of a contaminated aquifer such that groundwater samples could be obtained from closely spaced vertical sampling intervals. Such closely spaced groundwater sampling was required to gather geochemical evidence for intrinsic microbial degradation of hydrocarbons, to confirm the role of mineral weathering in aquifer as the source of ions responsible, and to demonstrate the link between the ionic concentration of the groundwater and the increased conductivity.

In a companion study (Legall, 2002) we have provided evidence for intrinsic biodegradation of hydrocarbons at the site by documenting the nature and extent of redox processes and zonation in the contaminated aquifer using the vertical variation in terminal electron acceptors (TEAs), DIC, and the $\delta^{13}C_{DIC}$. Depth distribution of TEAs and educts indicated that at the plume margins where RDH occur, SO_4 reduction has supplanted denitrification via dissimilatory nitrate reduction, and the reduction of Fe (III) and Mn(IV) as the major redox process. Within the portion of the aquifer with RDFH, the $\delta^{13}C_{DIC}$ values indicate that methanogenesis is the dominant redox process. These redox zones were identified as sites where changes in the pore water chemistry and the physical and chemical attributes of the aquifer minerals were likely to occur because of enhanced microbial activity. High soil conductivities also were measured in these zones.

The present paper is focused on: (a) providing evidence for mineral weathering in the aquifer by assessing the contribution of major ions derived from mineral-water reactions that result from in-situ geochemical and biogeochemical processes; and (b) documenting in a field setting how vertical changes in the groundwater chemistry (major ions, DIC, and stable isotopes) co-vary with bulk conductivity in contaminated and uncontaminated groundwater. We seek in this initial effort to unravel the complex role geochemical and microbial processes play in controlling the geochemistry of the groundwater at this site. We employ a novel concept based on the use of bulk conductivity measurements, major ion chemistry, the concentration of DIC, and the $\delta^{13}C_{DIC}$ to define broad chemical zones within the aquifer. The link between $\delta^{13}C_{DIC}$ and the bulk conductivity in contaminant plumes has to our knowledge, never been documented in the literature. The study represents some of the first steps taken to describe the relationship in detail.

The key to elucidating the role that geochemical and microbial processes play in influencing the groundwater chemistry lies in combining the information on the bulk conductivity of the aquifer media and the $\delta^{13}C_{DIC}$. These two seemingly disparate variables are related in a fundamental way. They both measure the combined effects of a number of integrated geochemical and biogeochemical processes that occur in both soil and groundwater. Thus their signatures are linked by processes and are imprinted on the host media.

The Relationship Between Conductivity and Biodegradation via Pore Fluid Chemistry

The basis for the use of electrical resistivity methods to detect LNAPL contamination of soil is dependent on the contrasting electrical properties of LNAPLs versus the pore fluids and groundwater displaced by LNAPL plumes. According to Archie's law, the electrical conductivity of clean geologic material (in the absence of clays) is described by (Archie, 1942):

$$\sigma_e = \sigma_w / (a\phi^{-m} S_w^{-n}) \quad \text{.....(1)}$$

Where σ_e is the effective (bulk) conductivity of the medium that is measured, ϕ is the fractional pore volume (porosity), S_w is the fraction of the pores containing fluid (i.e., water saturation), σ_w is the conductivity of the fluid, a is an empirical factor, n is a saturation coefficient (between 0.6 to 1.0), and m is a cementation factor (<1.5 for poorly cemented formations). The cementation and saturation exponents include information about pore structure and fluid distribution. If the subsurface porosity (ϕ) is assumed to be constant, the bulk conductivity (σ_e) can change if pore fluid conductivity (σ_w) or the saturation (S_w) varies. In fully saturated formations $S_w = 1$, and assuming constant porosity, the pore fluid conductivity (σ_w) becomes the important variable controlling the bulk conductivity. However, the pore fluid conductivity (σ_w) is directly linked to the total dissolved solids (TDS) contained in the water because most solutes in natural waters are ionic when in a dissolved state

(Stumm and Morgan, 1995). In general, the conductivity increases as TDS increase.

Typically, in routine field investigations, specific conductance (SpC) (the temperature-corrected conductivity) and TDS are measured using multi-parameter probes and are generally found to be a good measure of the ionic content and to reflect the electrical properties of the groundwater (Hem, 1985). Ions that contribute the most to SpC include: Ca^{2+}, Mg^{2+}, Na^{+}, K^{+}, HCO_3^{-}, SO_4^{2-}, NO_3, and Cl^{-}. Major inorganic ions typically reflect the products of various chemical reactions occurring within groundwater. Thus, it is expected that areas of active hydrocarbon biodegradation will be accompanied by enhancement of mineral dissolution due to the leaching action of acids that are generated in the process (Cozzarelli et al., 1990; Bennett et al., 1993; McMahon et al., 1995). Hence, enrichment of ions will occur within the contaminated groundwater relative to background locations. TDS and SpC are bulk measurements of the fluid property, thus they should be positively correlated with the bulk conductivity of the soil and serve as an indirect link between the bulk electrical properties of the soil and biodegradation.

Study Site

The site is an inactive petroleum refinery located in Michigan (Figure 1). It occupies approximately 13.2 hectares and is bounded to the north by a cemetery, to the west by a stream (Fish Creek and its associated wetlands), and on the south by a City Park, which is mostly wooded. Historical releases from tanks and pipelines resulted in the seepage of hydrocarbons into the subsurface, impacting soils and groundwater

beneath the main refinery site, the cemetery and the city park. The area investigated in this study lies entirely within the city park. Within the contaminated portion of the aquifer, different phases of hydrocarbon impact are recognized, namely, zones where residual and dissolved phase hydrocarbons (RDH) occur and zones where these phases coexist with free product (RDFH). The shallow stratigraphy at the site is characterized by approximately 4.6 to 6.1 m of fine to medium glacial outwash sands, coarsening below the water table to gravel and underlain by a 0.6 to 3.1 m clay aquitard (Dell Engineering, 1992). The mineralogy of the aquifer is predominantly quartz with minor amounts of albite and anorthite above the water table. However, below the water table, calcite, gypsum, and dolomite occur. Depth to the water table varies from 0.6 m to 0.9 m west to 4.6 to 5.8 m in the eastern portion of the study area. Groundwater levels vary up to 90 cm annually at the site (Atekwana et al., 2000; Werkema et al., 2000). Groundwater flows west-southwest towards Fish creek (Fig. 1) with a hydraulic gradient of 0.0015 m/m and a velocity of 1.68 m/day (Dell Engineering).

Material and Methods

The study site has been instrumented at several locations with vertical resistivity probes (VRP's) for measuring soil resistivity, a water table monitoring well, and multilevel piezometers (MLP's). Details of the VRP installation, resistivity measurements, and results are presented in Werkema et al., (2000) and Werkema (2002). Monitoring wells and multilevel piezometers were installed using a

Geoprobe™ drill rig. The water table monitoring wells were constructed of 2.54-cm PVC casings fitted with 152 cm slotted PVC screens and screened across the water table. The multilevel piezometers were constructed of flexible polypropylene tubing with six-inch nylon screens at vertical intervals of about 30 cm. The small tubes were bound to the outside of the 0.5–inch Schedule 80 PVC pipe with a 15.2 cm screen at the base. The piezometers were installed from the base of the aquifer into the vadose zone to document the steep soil conductivity gradients and to accommodate seasonal fluctuations in the water table.

Multi-level piezometers were sampled with a peristaltic pump using "low-flow" sampling techniques. Groundwater samples were collected from sample tubing screened below the water table. During pre-sampling purging, pH, SpC, and temperature of the purge water was measured and recorded. Field measurements of pH, temperature, salinity, TDS, and specific conductance were conducted with a HydroLab Minisonde™ multi-parameter probe. Alkalinity as bicarbonate was measured by potentiometric titration using 1.5 N H_2SO_4 to an acid equivalent point of 4.5 (Hach, 1992). Samples collected for major cations were filtered in the field using a 0.45µm pore size in-line-filters (Gelman Sciences, Inc.) prior to collection in acidified, 250 ml polypropylene bottles. Samples for major anions were collected in unacidified 250 ml polypropylene bottles. Major ions were analyzed using a Dionex DX 500 ion chromatograph. Silica was measured by the silicomolybdate method using a Hach DR/890 colorimetry kit (Hach, 2000). Elemental concentrations (Fe, Mn) were determined using a Leeman Labs P950 Inductively Coupled Plasma-

Atomic Emission Spectrometer (ICP–AES) equipped with a CETAC Corp. AT5000+ ultrasonic nebulizer.

For DIC and carbon isotopic analysis, 10 ml of water was collected and the CO_2 extracted using a modification of the gas evolution extraction technique (Atekwana and Krishnamurthy, 1998). CO_2 yields from water samples were used to determine the DIC concentrations reported in mg C/l. Isotope measurements were made using a Micromass Isotope Ratio Mass Spectrometer at Western Michigan University, Kalamazoo, MI, USA and are reported in the δ notation where:

$$\delta^{13}C\ (‰) = ((R_{sample}/R_{standard}) - 1) \times 10^3$$

R is $^{13}C/^{12}C$. $\delta^{13}C$ values are reported relative to VPDB. Routine $\delta^{13}C$ measurements have an overall precision of better than 0.1‰.

Results

The results of the bulk soil conductivity, geochemical and isotopic analyses for June 2000 are presented in Table 1. All of the data presented was obtained from the saturated zone. Bulk soil conductivity was initially recorded as resistivity. In this study, the resistivity is presented as its reciprocal, the bulk conductivity, in milliSiemens per meter (mS/m). The bulk soil conductivity represented is the average of conductivity readings from within the screened interval. Depth profiles of bulk conductivity and major ions are presented from an uncontaminated portion of the aquifer (MLP-9, Fig. 2a), portions of the aquifer contaminated with RDH (MLP-3,

Fig. 2b and MLP-10, Fig. 2c), and with RDFH (MLP1, Fig. 2d, MLP-5, Fig. 2e, and MLP-8, Fig. 2f). Specific conductance, inorganic ion concentrations, DIC and $\delta^{13}C_{DIC}$ are placed alongside the bulk conductivity profiles.

Bulk Conductivity

Bulk conductivities ranged from 3.5 to 18 mS/m in the uncontaminated portion of the aquifer. In MLP-9 the bulk conductivity increased sharply from an initial value of ~3.5 mS/m at top of the saturated zone (225.5 m) to a maximum of 18 mS/m at 224.5 m, thereafter it remains relatively constant then decreases slightly to 16 mS/m to the base of the aquifer (Fig. 2a). Within the contaminated zones bulk soil conductivities were also generally lower at the top of the saturated zone. Bulk soil conductivity ranged from 10 to 25 mS/m at MLP-3 and MLP-10 (Fig. 2b and 2c) located in the portion of the aquifer with RDH. At MLP-3, the bulk soil conductivity at the top of the water table (226.0 m) was ~9 mS/m and increased sharply to a maximum of 25.5 mS/m within a vertical distance of 1 m, then decreased to 20.5 mS/m at 223.8 m and recovered to 22.5 mS/m at the end of the profile. In MLP-10, the bulk soil conductivity increased from 6.8 mS/m at the top of the water table (225.5m) to 18.7 mS/m within 0.75 m, and remained relatively steady before decreasing to 14.8 mS/m at 223.9 m, remaining constant to the base of the profile.

At locations with RDFH, bulk soil conductivity ranged from 12 to 32 mS/m. At MLP-1 the bulk soil conductivity increased rapidly from 17 mS/m at the top of the aquifer (225.2 m) to 30 mS/m at 224.7, remained nearly constant to 222.8 m then

decreased to ~25 mS/m before increasing to 29 mS/m at the base of the profile (Fig. 2d). Within a vertical distance of 1.3 m from the top of the aquifer, the bulk soil conductivity for MLP-5 increased from ~12 mS/m to 30 mS/m, then decreased to ~20 mS/m at depth (Fig. 2e). Steep conductivity gradients characterize the irregular outline of the bulk soil conductivity curve for MLP-8 (Fig. 3f), which shows an overall increase with depth from ~13 mS/m at the top of the profile to 17 mS/m at the base of the profile.

Distribution of Water Quality Parameters

Generally, pH was higher (>7) at the uncontaminated location compared to the contaminated locations. At the contaminated locations the pH was < 7 but generally increased towards the base of the aquifer. Except for MLP-10, temperature was generally higher at contaminated locations compared to background (Table 1). The SpC was generally lower at the top of the aquifer and increased with depth at both contaminated and contaminated locations (Figs. 2g-l). On the average, SpC was greater at contaminated locations reaching maximum values of 1112 µS/cm at MLP-10 compared to a maximum value of 875 µS/cm at the background location. The TDS data showed the same trend observed for the SpC. Low TDS at the top of the aquifer was followed by a sharp increase with depth. TDS from uncontaminated groundwater ranged from 49.8 to 526.0 mg/L and from 83.6 to 711.8 mg/L at contaminated locations. Chloride was lowest at the top of the aquifer and increased

towards the base of the aquifer at both contaminated and background locations (Table 1).

Distribution of Major Ions, Alkalinity, DIC and $\delta^{13}C_{DIC}$

Overall there is spatial and vertical variability in the concentration of major ions across the site (Table 1). Groundwater at the contaminated locations showed a relative enrichment of most ions compared to background. There was a general increase in Na, Ca, Mg, and Si at the contaminated locations relative to background that is consistent with the weathering of the aquifer material (Table 1, and Figs. 2m-r, 2s-x, and 3g-l). Alkalinity and DIC were lowest at the top of the aquifer (Table 1, and Fig 3m-r). Generally, higher alkalinity and DIC occurred in the middle of the aquifer at most locations, coincident with zones of maximum bulk soil conductivities. Some ions (e.g. chloride) showed a marked increased towards the base of the aquifer (Table 1). Steep conductivity and concentration gradients exist at or close to the top of the aquifer where chloride concentration indicate dilution of groundwater is occurring and also at the base of the aquifer due to stratification of the groundwater. The $\delta^{13}C_{DIC}$ for groundwater at the uncontaminated location (MLP-9) ranged from –14.6 to –12.3‰ and decreased slightly with depth (Figs. 3s). At the contaminated locations the $\delta^{13}C_{DIC}$ was more negative at the top of the aquifer (–24.2 to –16.9‰) and generally more positive at depth (Fig. 3t-x). Negative $\delta^{13}C_{DIC}$ values in the range of –11.3 to –16.8‰ were encountered below the water table in MLP-3 and 10, locations with RDH (Figs. 3t-u). In general, more positive $\delta^{13}C_{DIC}$ values were

observed in groundwater at locations with RDFH (Figs. 3v-x). The $\delta^{13}C_{DIC}$ reached a maximum of +6.5‰ in MLP-5 (Fig.3w).

Discussion

The basic premise of this study is that the presence of conductive zones within hydrocarbon plumes is a result of enhanced weathering processes that are driven by bacterially mediated reactions that occur during hydrocarbon degradation. In general, mineral weathering is driven by CO_2 produced within the soil zone. Under natural conditions, soil CO_2 is incorporated in recharge water infiltrating through the vadose zone prior to entering the saturated zone. This dissolved CO_2 in the form of carbonic acid acts as a primary weathering agent and minerals with high solubility are readily dissolved in the aquifer. Bacterial degradation of hydrocarbons augments the supply of CO_2 in the aquifer and in addition produces organic acids that further enhance mineral weathering (Hiebert and Bennett, 1992; McMahon et al., 1995; Ullman and Welch, 2002). Thus mineral dissolution increases the ionic strength of the pore fluid resulting in an increase in the bulk conductivity of the sediments.

Evidence for Mineral Weathering

In the aquifer under study, the mineralogy consists primarily of quartz sand with minor quantities of calcite and dolomite, and residual amounts of Na-rich and Ca-rich plagioclase. Based on the mineralogy of the aquifer we expect to see enrichment of Na, Ca, Mg and Si as a result of the weathering of these aquifer

minerals by aggressive CO_2-rich groundwater and organic acids (Bennett et al. 1993; Stumm and Morgan, 1995; Herczeg and Edmunds, 2000). Furthermore enhanced dissolution of these minerals should also be accompanied by an increase in HCO_3, which should be reflected in the alkalinity, and DIC. Additionally, because of the increased contribution of CO_2 from microbial degradation of hydrocarbons within the contaminated portions of the aquifer we should expect to see evidence for increased CO_2 production at the contaminated locations that should be reflected in the DIC. This is consistent with the elevated alkalinity (30 to 547 mg/l) and DIC (27 to 206 mg C/l) observed within the contaminated regions of the aquifer relative to background alkalinity (90 to 320 mg/l) and DIC (29 to 87 mg C/l).

Evidence for mineral weathering in the aquifer is derived from several sources. We use variations in the ionic ratios in the contaminated groundwater compared to background as evidence to support increased contribution of these ions to the groundwater. We use this approach instead of comparing total ion concentrations because some of the complex water-rock interactions that govern the uptake or release of ions in the aquifer during weathering are not strictly controlled by solubility (Herczeg and Edmunds, 2000).

The Ca:Mg ratio of the groundwater increased in the contaminated portions of the aquifer compared to background. At the background location the Ca:Mg ratio ranged from 1.9 to 2.5. However, in the locations with RDH the ratio ranged from 1.9 to 5.9 in MLP 3 and from1.9 to 4.6 in MLP 10. At the locations with RDFH, the Ca:Mg ratio ranged from 8.2 to 10 at MLP-1, from 2.2 to 3.0 in MLP-5, and from 2.8

to 5.1 at MLP-8. The trend of increasing Ca:Mg ratios in the contaminated portions of the aquifer is indicative of enhanced production of these ions in the aquifer relative to background.

In order to investigate increases in Na, we use a plot of Na versus Cl (Fig. 4) to indirectly assess the contribution of Na to the groundwater from the dissolution of albite. We assumed a 1:1 stoichiometric relationship between Na and Cl in the groundwater assuming that Cl is balanced primarily by presence of Na in the aquifer. Groundwater from MLP-1 and 5, locations with RDFH, and a sample from MLP-3, located in the portion of the aquifer with RDH, plot above the 1:1 line indicating the presence of excess Na, which suggests that a likely source of additional Na is from the dissolution of plagioclase. The remaining groundwater samples plot below the 1:1 line, which may suggest Cl contributions to the groundwater from road salt or Na removal from the groundwater by interactions with clays produced through mineral weathering (Herczeg and Edmunds, 2000).

Elevated concentrations of dissolved Si in the contaminated portions of the aquifer compared to background provide additional evidence for mineral weathering in the aquifer. Groundwater samples in the uncontaminated portions of the aquifer have dissolved Si ranging from 8 to 11 mg/l. In the portion of the aquifer contaminated with RDH dissolved Si ranged from 10 to 17 mg/l and was higher (13 to 26 mg/l) in the portion of the aquifer with RDFH (Table 1). Hence, compared to uncontaminated locations, the groundwater in contaminated portions of the aquifer appears to have been altered by the contribution of ions from the weathering of

carbonate and silicates present in the aquifer.

The Link Between TDS and Bulk Soil Conductivity

The relationship between the major ions released during the weathering of aquifer minerals and the measured TDS is a key step in linking the TDS to the bulk conductivity. In order to document the relationship between the TDS and the major ion chemistry we first examined a plot of the TDS and the dominant ions (Na+Ca+ Mg+HCO_3) represented in the weathering reactions to evaluate the relationships suggesting that ionic contribution via weathering reactions contributed to groundwater TDS and as a result affected the conductivity (Fig. 5). The correlation between these variables for the different MLPs is summarized in Table 2. Overall strong positive correlations between the TDS and the major ions were apparent ($0.99<r^2>0.66$; $0.09<p>0.0002$). In spite of the relatively few data points for correlation, we contend that most of the TDS can be related to the enrichment of ions resulting from enhanced mineral dissolution and it is this enrichment that is causing the enhancement in current flow. Although other ions (e.g. SO_4 and NO_3) present in the aquifer also contribute to the TDS, we argue that several of these ions owe their continued presence in the aquifer to redox processes and compared to the dominant ions, their contribution to TDS is small. This is consistent with our correlation, which indicates that most of the TDS can be accounted for by the presence of Na, Ca, Mg, and HCO_3, the ionic products of mineral weathering in the aquifer.

In porous geologic media, current flow is mostly electrolytic indicating that a

positive correlation should exist between bulk conductivity and TDS. Bulk conductivity data were plotted against TDS for each sampling location (Fig. 6) and the relationships statistically analyzed (Table 2). Groundwater from the background location (MLP-9) showed a positive correlation between bulk conductivity and TDS (Fig. 7). This relationship is described by the least squares regression equation: Bulk Conductivity = 0.058 (TDS) – 13.35, r^2=0.88. Furthermore, groundwater from MLP-3, with RDH also showed a positive correlation between bulk conductivity and TDS. This relationship (not shown in Fig. 6) is described by the least squares regression equation: Bulk Conductivity = 0.027 (TDS) + 6.10, r^2=0.93. The positive correlations are also consistent with relationship between the bulk conductivity and major ions at these locations (Table 2) and suggest that the TDS was responsible for the bulk conductivity at these locations.

However, groundwater from MLP-10, also located in a portion of the aquifer with RDH showed poor correlation between bulk soil conductivity and TDS (Table 2; Fig. 6). Moreover, the bulk soil conductivity from MLP, 1, 5 and 8, locations with RDFH showed no apparent correlation with TDS (Table 2; Fig. 6). This apparent lack of correlation between bulk soil conductivity and TDS at contaminated locations suggests that the positive linear relationship between bulk soil conductivity and TDS may not be valid in contaminated settings. Thus TDS may not reliably predict the bulk conductivities of hydrocarbon-impacted soils. Additionally, based on the data presented in Table 1, it is important to note that the highest TDS were not always coincident with the highest bulk soil conductivity. For example, the highest recorded

TDS is at MLP-3 and 10, however, the highest recorded bulk soil conductivities are recorded at MLP-1 (Table 1). These results suggest that bulk soil conductivities measured at the contaminated locations, notably at MLP-1, 5, and 10 were not dominated by pore fluid conductivity, thereby suggesting another mechanism of conduction at these locations or that other constituents in the groundwater, such as organic acids, not recorded by the TDS, may play a role in determining the bulk soil conductivity.

Conduction of electricity through porous media occurs by two mechanisms. The primary mode is by the movement of ions through the bulk fluid, the other occurs as surface conduction by adsorbed ions moving along the surfaces of pores and small fractures (Wildenschild et al., 1999). Assuming that current flow through the soils was mainly electrolytic, it appears that two mechanisms of conduction may exist within the uncontaminated and contaminated regions of the aquifer: a region where the ionic strength of the saturating fluid controlled conduction and a region dominated by surface conduction. If this is true then it possible that surface conduction might be an important conduction path at contaminated locations and probably linked to microbial processes and subsequent geochemical transformation of the mineralogy and pore fluid chemistry occurring within the aquifer.

It is well documented that surface conductivity can occur along surfaces of mineral grains (e.g. Knight and Endres, 1990; Lesmes and Morgan 2001). Hydrocarbon degradation may produce charged organic species (e.g. volatile fatty organic acids (VOAs) such as acetic acids (e.g. Cozzarelli et al., 1990; McMahon et

al., 1995) and biosurfactants (Cassidy et al., 2001; 2002). These charged organic species could attach to grain surfaces resulting in interfacial polarization thus enhancing surface conduction at the mineral-fluid interface (Stumm, 1992). At the study site, previous investigations have documented the presence of organic acids at MLP 1 and 5, locations with free phase hydrocarbons, but organic acids were not measured at MLP-3, with RDH or at MLP-9, at the background location (Atekwana et al., 2002). Biosurfactants have also been identified at the contaminated locations (specifically at MLP-1 and MLP5), but were not measured at MLP-9 (Cassidy et al., 2002). Organic acids and surfactants have a charge at their surface and can attract positively charged ions polarizing the subsurface, analogous to membrane polarization effects that are observed in clays (Scholl and Harvey, 1992). Furthermore, bacteria have negatively charged surfaces that can also attract positively charged ions, thus polarizing the substrate (Wasserman and Felmy, 2000). Thus the mineral-water interactions that govern the supply of ions either through dissolution/precipitation reactions or by the generation of charged organic species have their origin in microbial processes that interact closely with geochemical transformations. Thus, further knowledge of biogeochemical processes occurring in contaminated aquifers may be an important key to understanding the nature and distribution of the surface conduction phenomenon.

Evidence for Geochemical Process From $\delta^{13}C_{DIC}$ and Bulk Conductivity Signatures

The key to elucidating the role that geochemical and microbial processes play

in influencing the groundwater chemistry lies in combining the information on the bulk conductivity of the aquifer media and the $\delta^{13}C_{DIC}$. These two seemingly disparate variables are related in a fundamental way. They both measure the combined effects of a number of integrated geochemical and biogeochemical processes that occur in both soil and groundwater. Thus their signatures are linked by processes and are imprinted on the host media.

To explain the lack of correlation between the TDS and bulk soil conductivity we reasoned that the bulk soil conductivity measures the cumulative effect that geochemical processes have on the aquifer media (both soil and ground-water), and the $\delta^{13}C_{DIC}$ provides insights into the nature of the processes. Therefore, these two variables record the effect of geochemical processes on the host media. Thus as aquifer solids undergo transformation by dissolution and precipitation reactions and as the geochemistry of the associated pore water evolves in response to these changes a permanent record of these alterations is conveyed in the bulk soil conductivity measurements. Thus, the bulk soil conductivity is an intrinsic property of the media and is ideally suited for discerning changes in bulk water chemistry based on total solute concentrations, which is normally reflected in the ion concentrations. On the other hand, the $\delta^{13}C$ tends to behave fairly conservatively as it monitors carbon flows in contaminated and uncontaminated aquifers that occur via redox reactions. Its greatest advantage is that it can, in some instances, clearly distinguish the type of redox process occurring in the system. Thus clues to the understanding of the nature of the relationship between the bulk soil conductivities observed in contaminated

portions of the aquifer and the groundwater chemistry, as a first approximation, could be derived by careful examination of the bulk soil conductivity and the $\delta^{13}C$ data.

A cross-plot of the $\delta^{13}C_{DIC}$ and bulk conductivity data is presented in Fig. 7. The plot was not meant to demonstrate the dependence of bulk conductivity on the $\delta^{13}C_{DIC}$ rather it was used to show the magnitude of isotopic separation for the bulk conductivity data. The data falls into three groups consisting of: 1) recharge waters from the top of the aquifer in the contaminated portions of the aquifer characterized by low bulk conductivities (3.5 to 15 mS/m) and very negative $\delta^{13}C$ values (–21 to –25‰) (Group I); 2) groundwater from both uncontaminated and contaminated portions of the aquifer with bulk conductivities ranging from 10 to 25 mS/m and $\delta^{13}C$ values ranging from –16.9 to –9.5‰ (Group II); and 3) groundwater from contaminated wells (MLP-1 and 5) containing free product with bulk conductivities ranging from 12 to 32 mS/m, and higher $\delta^{13}C$ values ranging from –4.4 to +6.5‰ (Group III). These groups represent groundwater linked by distinct redox processes operating in the aquifer (Legall, 2002).

Redox reactions that facilitate hydrocarbon degradation generate CO_2, which contributes to mineral weathering and increases the TDS and DIC. It is this property, common to redox reactions that provide the unique approach for establishing the link between the bulk soil conductivity and the $\delta^{13}C_{DIC}$. On the other hand, bulk soil conductivity through its relationship to TDS records the effect of those processes. Therefore, to further examine the groundwater chemistry and its relationship to the bulk conductivity and to assess major ion contribution to the bulk conductivity we

plotted the $\delta^{13}C_{DIC}$ against the DIC (Fig. 8). We used this approach to better understand the spatial variations in geochemical processes affecting the groundwater chemistry. The data clustered into three groups similar to that observed in Fig. 7. These groups have been previously described (Legall, 2002). We contend that the similarity between these cross-plots is based on process-driven biogeochemical changes that collectively increased the DIC and TDS and as we demonstrated earlier, the increase in TDS resulted in the high bulk conductivities. We infer that the various groupings delineated on the basis of the $\delta^{13}C_{DIC}$ and bulk conductivity, and DIC may represent sequential stages in a continuum of redox processes associated with microbial hydrocarbon degradation in the aquifer.

Specifically we note in Fig. 8 that background groundwater from the study area has DIC and $\delta^{13}C_{DIC}$ values close to that for uncontaminated groundwater from southwest Michigan. Groundwater from Group II is influenced by a range of microbial processes including aerobic respiration at background locations, and redox processes such as the reduction of NO_3, Mn(IV), Fe(III), and SO_4 at contaminated locations. Within the contaminated zones, the increase in CO_2 due to microbial hydrocarbon degradation increases the DIC, hence, the groundwater DIC evolves along a path parallel to the x-axis (Fig. 8).

CO_2 Control on the Weathering Processes

In order to demonstrate CO_2 control on the weathering processes, we plot the sum of the concentration of Ca and Mg versus DIC (Fig. 9). We use Ca and Mg

because they represent the dominant cations in groundwater at the site (Table 1) and the fate of these ions is controlled by reactions involving carbonate. Generally groundwater DIC increases with increasing Ca+Mg (Fig. 9). Groundwater in Group I (Fig. 8) is derived from MLP-3, MLP-5, and MLP-10, located in contaminated portions of the aquifer. The groundwater occurs at different locations but share one common feature, they occur close to or at the top of the water table. These waters are associated with recharge and have low Ca+Mg and DIC (Fig.9). In the contaminated portions of the aquifer these waters are in contact with residual phase contamination or free product at the top of the water table. The low DIC negative $\delta^{13}C$ values (–26 to –28‰) suggest that the groundwater within this group may not have had sufficient time to interact with aquifer solids (not enough time for dissolution), and is likely a mixture of water and hydrocarbons. With increasing depth, both Figs. 8 and 9 suggest that groundwater DIC and $\delta^{13}C$ may evolve through dissolution of the aquifer minerals as a result of mineral weathering induced by microbial activity.

Groundwater in Group II (Fig. 8) derived from MLP-1, MLP-3, MLP-8, MLP-9, and MLP-10, within uncontaminated and contaminated portions of the aquifer exhibits a wide range of DIC (30 to 206 mg C/l) with $\delta^{13}C_{DIC}$ values ranging from –16.9 to –9.5‰. MLP-9 reflects background conditions, however, in several MLPs, notably MLP-3, 8, and 10, the reduction of NO_3, Fe(III), Mn(IV) and SO_4 have been identified as important redox processes occurring within the contaminated zone at these locations (Legall, 2002).

Within Group II, the increase in CO_2 due to microbial hydrocarbon

degradation increases the DIC, hence, the groundwater DIC evolves along a path parallel to the x-axis (Fig. 8). Uncontaminated groundwater (MLP-9) has $\delta^{13}C_{DIC}$ values consistent with carbonate dissolution by soil CO_2 derived from soil organic carbon with $\delta^{13}C$ close to –27‰ (Legall, 2002). Of the Group II groundwater from RDH locations (MLP-3 and MLP-10), DIC and Ca+Mg at MLP-3 increase consistently to a maximum within the zone of greatest hydrocarbon impact indicated by higher bulk soil conductivity. A similar increase in DIC and Ca+Mg is also observed at MLP-10, except for groundwater at the base of the aquifer, which shows DIC and $\delta^{13}C_{DIC}$ close to background. Higher DIC at MLP-3 may be due to the predominance of redox processes such as NO_3, Mn(IV), Fe(III) reduction compared to SO_4 reduction at MLP-10 (Legall, 2002). At MLP-8, a location with RDFH although Ca+Mg is comparable to that for contaminated groundwater within Group II, the DIC is not as high compared to most of the groundwater from contaminated portions of the aquifer (Fig 9). The low DIC may result from dilution by recharge water. The progression towards high DIC and Ca+Mg within zones with increasing $\delta^{13}C_{DIC}$ provides further evidence for groundwater DIC evolution in CO_2-carbonate controlled system and is consistent with groundwater chemistry dominated by the weathering of carbonate minerals.

Groundwater from MLP-1 and MLP-5, locations with RDFH, is associated with Group III and originates solely from a portion of the aquifer undergoing methanogenesis. Groundwater from MLP-5 shows a progressive increase in DIC and Ca+Mg throughout the zone of greatest hydrocarbon impact indicated by higher bulk

soil conductivity. On the other hand, groundwater from MLP-1 shows little variability in DIC and Ca+Mg (Fig. 9). This suggests that at MLP-1 the CO_2 produced during microbial hydrocarbon degradation is being consumed by reduction to CH_4. Further we suggest that Group III groundwater represent the terminal stage in the groundwater isotopic and DIC evolution.

The apparent evolution to methanogenesis or more positive $\delta^{13}C_{DIC}$ values also results in higher soil conductivity i.e., the more methanogenic the zone, the more conductive the zone. However, we also note the poor correlation between the bulk conductivity and TDS at locations where methanogenesis is the dominant redox process. We suggest that microbial activities that accompany hydro-carbon degradation under methanogenesis may significantly alter the aquifer matrix and pore water chemistry by regulating pH, facilitating redox reactions, producing organic acids, modulating dissolution/precipitation and adsorption/desorption reactions, and inducing complexation of ions with VOAs. Such processes are likely to contribute to surface conduction, which increases the bulk conductivity of the soils and may be responsible for the poor correlation with TDS.

Summary and Conclusions

Contaminated aquifers are perturbed systems where geochemical conditions are in disequilibrium and tendency for the system to attain a new equilibrium is regulated by external factors such as recharge and nutrient replenishment. This shifting equilibrium apparently gives rise to several important effects. Firstly, the

ionic concentrations of the groundwater change in response to inputs from in-situ geochemical and biogeochemical processes. Secondly, processes that are not yet clearly defined alter the aquifer matrix, changing its electrical properties, resulting in the anomalous conductive conditions observed in the geophysical measurements.

We contend that bulk conductivity measurements when used together with geochemical and isotopic analyses can provide important insights into the nature of geochemical processes operating in contaminated environments and perhaps in other hydrologic settings. The fact that this technique has been little used is not surprising because the ability to document the relationship relies on the acquisition of bulk conductivity measurements at closely spaced sampling intervals complemented with a geochemical sampling protocol that is guided by geophysical observation.

The ideas presented in this study have implications for geologists involved in site investigations requiring characterization and monitoring. From a geological standpoint, the integrated approach outlined in this study may be of interest to those who seek cost effective alternatives for site characterization and monitoring and to better understand the behavior of contaminant plumes in the surface. Site characterization and monitoring have relied on a network of monitoring wells, which as this study illustrates may not provide the spatial resolution necessary to assess contaminant distribution or its degradation. This study suggests that geoelectrical methods may be used as inexpensive and non-invasive sensors of subsurface hydrocarbon contamination. Such methods can be used to characterize the sub-surface at high resolution by delineating zones of high conductivities. This can be

followed by targeted confirmatory geochemical investigations using Geoprobe® borings or wells. From a geophysical perspective, the results of this study raise important questions regarding the effect of biogeochemical processes on geoelectric signatures observed in contaminated soils.

The materials and mechanisms that contribute to the changes in bulk conductivity during methanogenesis are largely unknown. Previous studies have demonstrated surfactant production in contaminated aquifers (Cassidy et al., 2002; Rosenberg and Ron, 1996) and the production and consumption of VOAs by microorganisms (McMahon and Chappelle, 1991; Cozzarelli et al., 1994; Routh et al., 2001). However, the role of surfactants and organic acids in altering the geoelectic signatures has not been investigated.

The role of bacteria in this process has also not been fully explored, although it is known that bacteria have a negative surface charge in the pH range of most natural waters and the presence of ionizable functional carboxyl, hydroxyl, and amino groups on their cell walls contribute to surface charge (Scholl and Harvey, 1992). These authors also suggest that the presence of Ca may enhance sorption by bacteria in contaminated water at higher pH, and that other factors including the ionic strength, pH, and the presence of divalent ions may determine the magnitude of electrostatic interactions between cell and surface.

Microbial colonization and metabolic activity has also been implicated in clay precipitation on anorthoclase (Bennett et al., 1996). The presence of clays on the surface of mineral grains can significantly alter the bulk conductivity. Ultimately

these complex interactions are expressed in the geoelectric response of the aquifer, however, the extent of these interactions and their relationships to the bulk conductivity are as yet unexplored.

These observations underlie the need to investigate aquifer solids in order to gain a better understanding of the processes and products that result from the geochemical and biogeochemical reactions at contaminated sites. We believe the link between the electrical properties of contaminated aquifers and the pore water chemistry within a framework of microbially induced degradation processes has long term implications for basic research into understanding the process of hydrocarbon biodegradation at contaminated sites.

Table 1. Bulk Conductivity of Soils, pH, Temperature, Alkalinity, SpC, TDS, Na, Mg, Ca, Si, Cl, DIC, and $\delta^{13}C_{DIC}$ Distribution in Groundwater From Multilevel Piezometers.

Well ID	Elevation (m)	Bulk Conductivity (mS/m)	pH	Temperature (°C)	Alkalinity (mg/l)	Specific Conductance (µs/cm)	TDS (mg/l)	Na (mg/l)	Mg (mg/l)	Ca (mg/l)	Si (mg/l)	Cl (mg/l)	DIC Conc. (mg C/L)	$\delta^{13}C_{DIC}$ (‰)
MLVL - 9	225.0	3.6	7.1	13.5	90.0	470.3	301.0	16.5	15.3	62.2	8.0	46.4	29.9	-12.3
(Uncont.)	224.6	18.4	7.3	12.4	258.0	771.9	494.0	44.7	29.2	106.9	9.0	107.5	71.2	-14.5
	224.1	16.1	7.1	11.7	311.0	851.6	545.0	24.7	39.5	129.3	11.0	51.8	84.7	NA
MLVL - 3	225.6	10.4	6.3	16.4	41.0	255.9	164.1	1.3	1.7	7.4	14.0	0.7	30.1	-24.2
(RDH)	225.1	23.6	6.4	15.3	431.0	947.5	606.5	5.0	19.5	189.9	10.0	5.7	170.6	-16.8
	224.7	25.4	6.5	14.4	547.0	1064.0	680.5	8.2	32.6	258.1	17.0	12.1	206.3	-13.3
	224.2	21.3	6.7	14.2	526.0	1030.0	659.4	24.9	37.5	191.0	13.0	24.2	153.3	-14.7
	223.8	21.2	6.8	13.1	420.0	919.9	589.5	25.4	35.3	154.5	11.0	40.2	107.7	-14.7
	223.3	22.2	6.5	13.7	333.0	910.4	582.1	18.5	48.1	149.5	12.0	47.2	86.7	-14.0
MLVL - 10	225.2	11.2	5.8	12.7	38.0	131.0	83.6	3.5	3.4	12.4	15.0	4.2	55.1	-22.2
(RDH)	224.8	20.0	6.1	12.5	210.0	474.0	305.0	5.3	8.4	47.0	11.0	14.3	114.0	-11.3
	224.3	15.3	6.5	12.4	401.0	766.5	491.6	11.3	20.5	155.7	13.0	27.8	150.5	-11.4
	223.9	14.9	6.6	12.0	524.0	1112.0	711.8	10.0	18.2	105.7	15.0	58.6	151.3	-15.3
	223.4	15.2	6.6	12.3	380.0	1026.0	655.9	29.1	52.6	161.2	13.0	70.1	99.0	-15.7
MLVL - 1	225.1	30.9	6.4	15.1	415.0	815.0	520.3	5.3	12.6	170.5	18.0	1.5	135.3	-16.9
(RDFH)	224.7	29.2	6.4	14.5	495.0	916.2	585.9	21.8	19.3	184.6	16.0	13.2	163.5	-1.9
	224.2	31.9	6.5	13.6	510.0	944.0	607.8	26.3	19.4	177.4	15.0	17.2	150.4	0.7
	223.8	32.2	6.5	14.3	515.0	945.8	609.4	28.1	19.5	177.0	16.0	17.5	154.9	0.5
	223.3	25.9	6.5	14.4	503.0	942.7	602.8	32.3	17.7	177.1	15.0	18.9	148.8	-0.8
	222.9	25.3	6.5	13.6	521.0	957.3	613.4	33.3	17.3	174.1	17.0	14.9	154.0	0.6
	222.4	29.6	6.6	15.5	496.0	934.6	599.4	47.8	28.9	141.7	22.0	34.7	139.8	1.8
MLVL - 5	225.0	15.2	6.1	19.1	30.0	185.4	118.6	3.3	2.4	20.2	14.0	1.0	45.0	-24.2
(RDFH)	224.5	23.2	6.4	FP	206.0	318.0	204.0	3.1	7.1	103.9	13.0	0.5	89.9	-1.3
	224.1	18.2	6.4	15.9	509.0	931.2	594.0	14.9	23.2	189.7	20.0	17.5	165.4	6.5
	223.6	17.7	6.7	17.1	469.0	891.2	570.7	22.6	32.5	153.1	20.0	30.7	126.1	-2.3
MLVL - 8	224.6	12.7	FP	FP	FP	FP	FP	1.3	3.6	14.6	15.0	1.1	27.0	-22.2
(RDFH)	224.1	17.5	6.9	13.8	232.0	577.0	367.7	8.0	14.5	71.1	14.0	15.2	64.2	-10.0
	223.7	17.6	7.0	13.9	441.0	941.2	585.0	21.3	34.5	155.7	19.0	46.2	114.1	-9.5
	223.2	16.5	6.9	15.3	437.0	978.3	624.8	23.6	42.8	162.6	16.0	55.0	108.5	-11.6
	222.8	18.6	6.9	14.5	418.0	996.5	638.8	24.5	44.1	163.6	16.0	59.1	102.8	-12.7

FP = Free Product NA = Not Analyzed Uncont. = Uncontaminated Location
RDH = Locations With Residual and Dissolved Phase Hydrocarbons RDFH = Locations With Residual, Dissolved and Free Phase Hydrocarbons
Elevation Data to the top of the Screened Interval

Table 2. Correlation Among Chemical Parameters From Multilevel Piezometers

Well ID		TDS vs $Na+Ca+Mg+HCO_3$	TDS vs Bulk Conductivity
MLP-9	Background	r^2=0.999 p=0.0009 n=3	r^2=0.884 p=0.2217 n=3
MLP-3	Dissolved and residual phase hydrocarbons	r^2=0.979 p=0.0002 n=6	r^2=0.932 p=0.0017 n=6
MLP-10	Dissolved and residual phase hydrocarbons	r^2=0.664 p=0.0927 n=5	r^2=0.048 p=0.7240 n=5
MLP-1	Dissolved, residual and Free Phase Hydrocarbons	r^2=0.951 p=0.0002 n=7	r^2=0.071 p=0.5623 n=7
MLP-5	Dissolved, residual and Free Phase Hydrocarbons	r^2=0.954 p=0.023 n=4	r^2=0.005 p=0.9284 n=4
MLP-8	Dissolved, residual and Free Phase Hydrocarbons	r^2=0.989 p=0.0051 n=4	r^2=0.003 p=0.9487 n=4

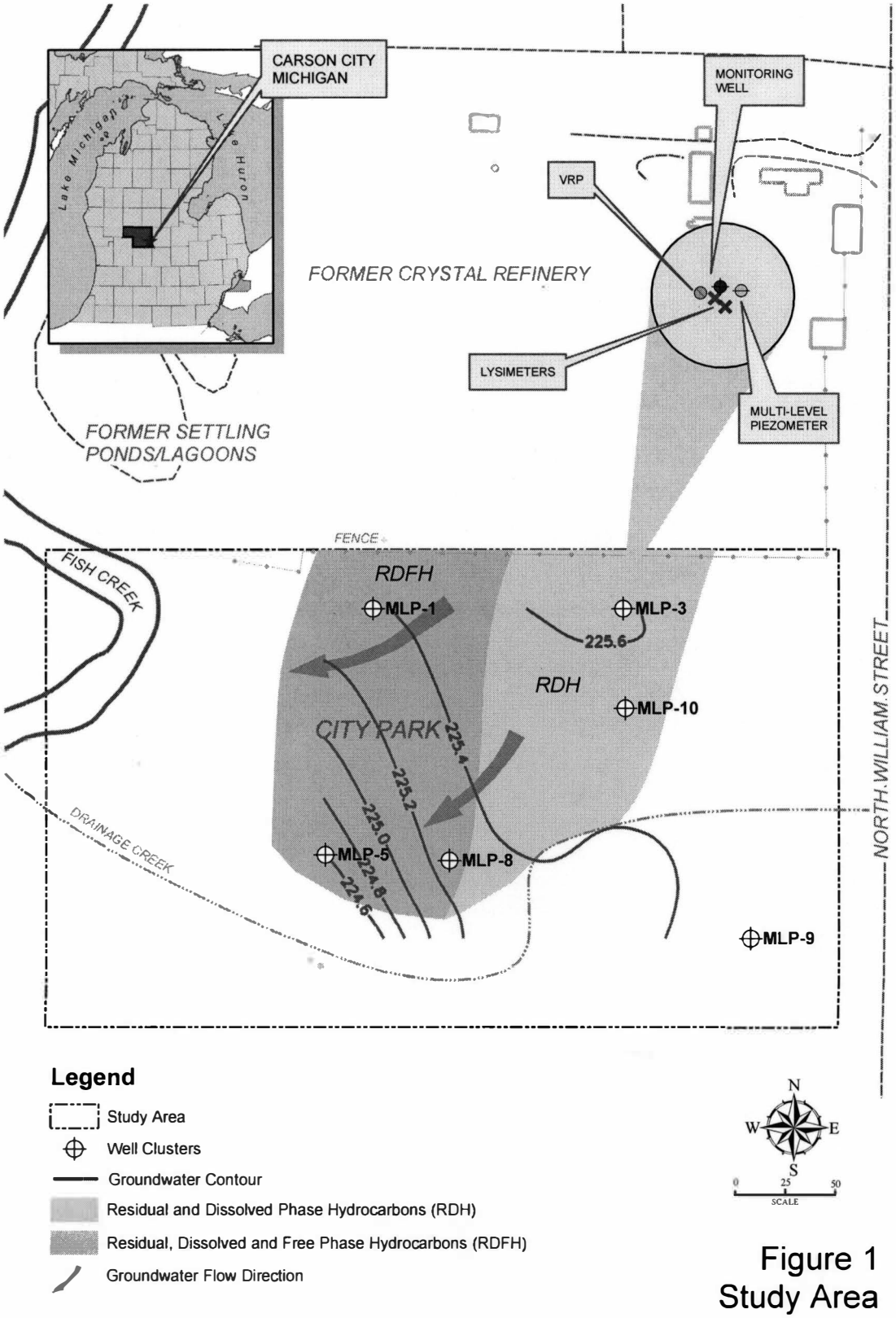

Figure 1
Study Area

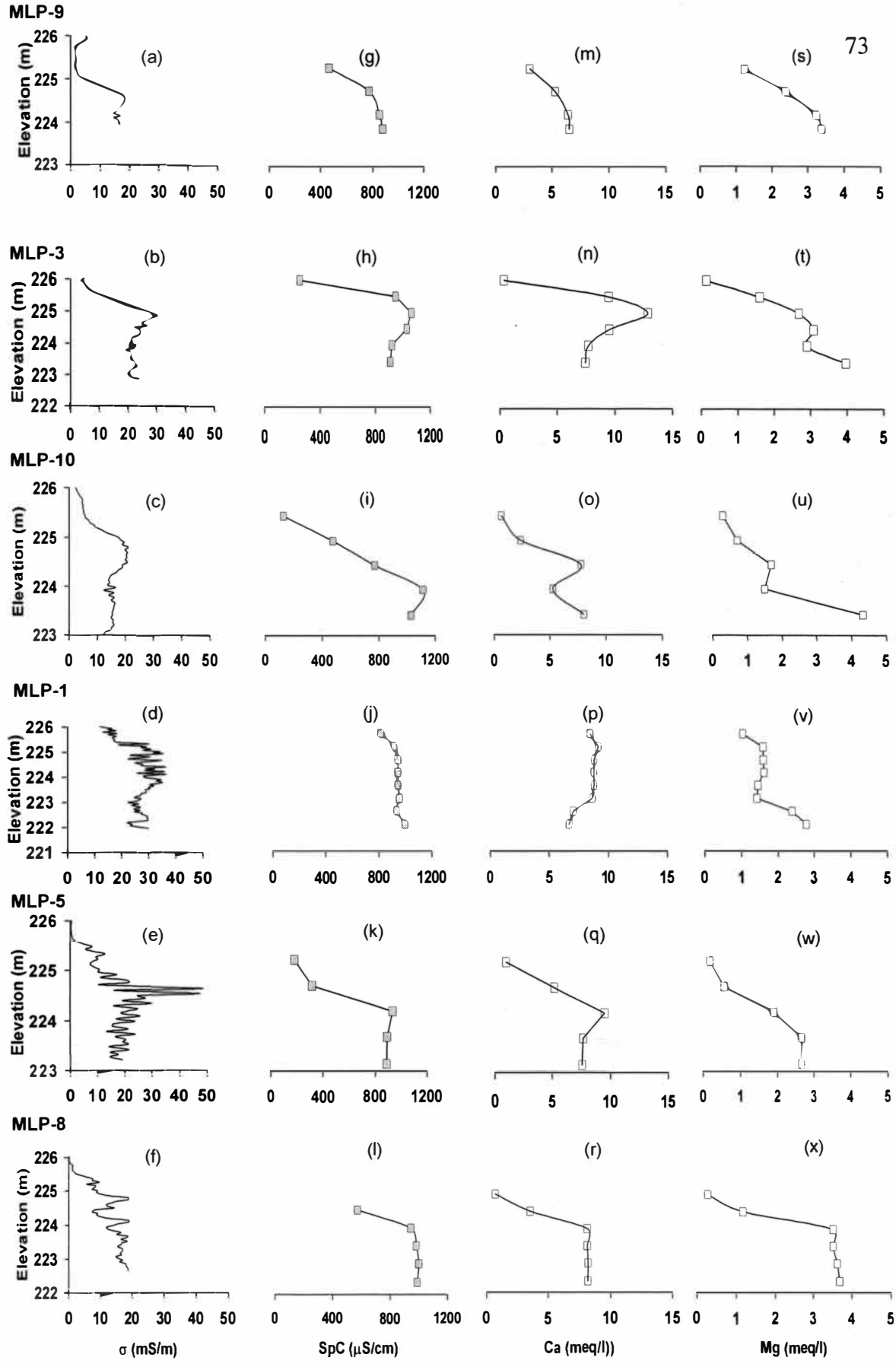

Figure 2. Vertical Profile of Bulk Conductivity of Soils, and SpC, Ca, and Mg in Groundwater for the Background Location (MLP-9), for Locations With Residual and Dissolved Phase Hydrocarbons (MLP-3 and MLP-10), and for Locations With Residual, Dissolved, and Free Phase Hydrocarbons (MLP-1, MLP-5, and MLP-8)

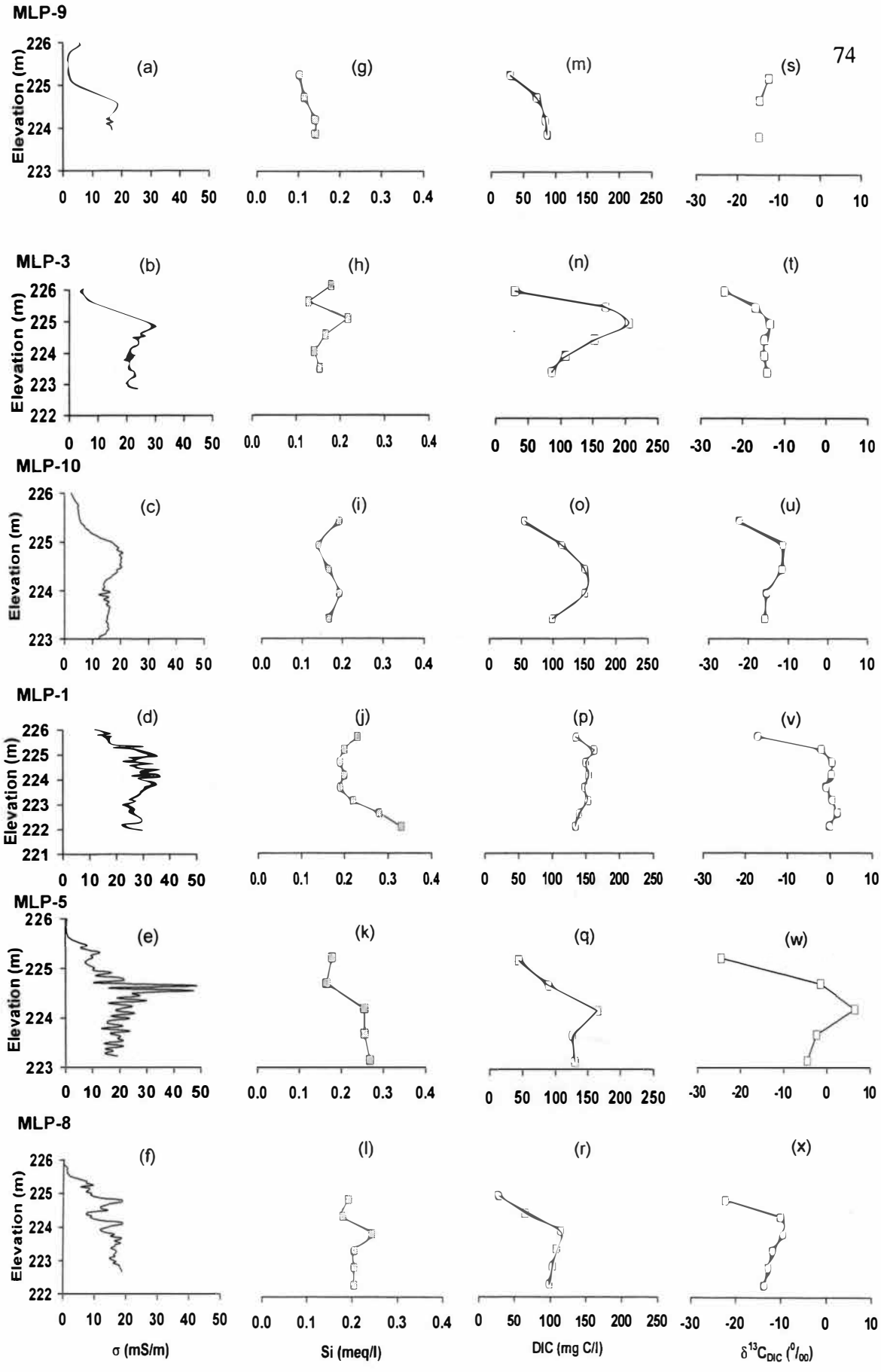

Figure 3. Vertical Profile of Bulk Conductivity of Soils, and Si, DIC, and $\delta^{13}C_{DIC}$ in Groundwater for the Background Location (MLP-9), for Locations With Residual and Dissolved Phase Hydrocarbons (MLP-3 and MLP-10), and for Locations With Residual, Dissolved, and Free Phase Hydrocarbons (MLP-1,

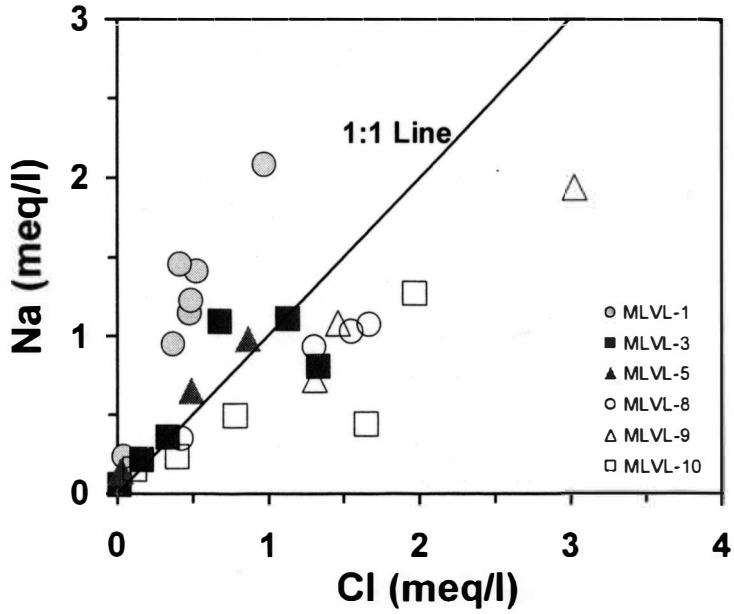

Figure 4. Na versus Cl for the Groundwater Samples. The Diagonal Line is the 1:1 Relationship Between Na and Cl. Units in Milliequivalents per Liter (meq/l).

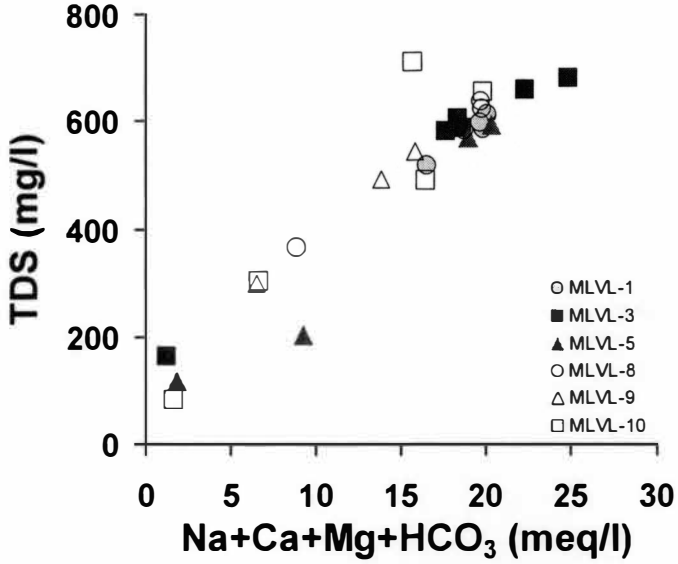

Figure 5. Cross Plot of Groundwater TDS and the Dominant Ions ($Na+Ca+Mg+HCO_3$) Derived From Mineral Weathering. Correlation coefficients for the Relationships at Each MLP Are Listed in Table 2.

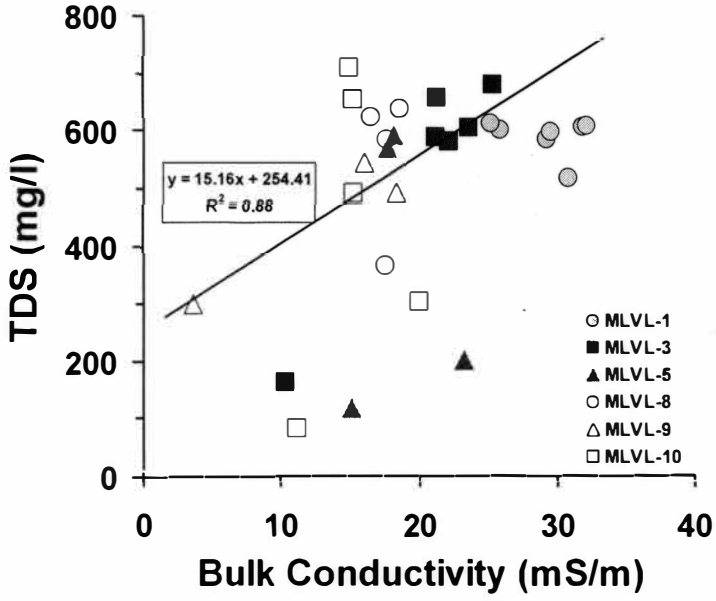

Figure 6. Cross Plot of Bulk Soil Conductivity and Groundwater TDS With the Least Squares Regression Line for Uncontaminated Groundwater. Correlation Coefficient for Regression is Listed in Table 2.

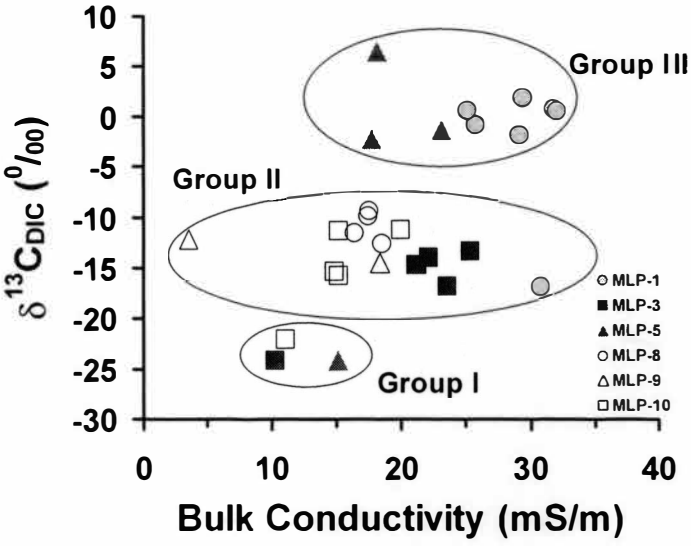

Figure 7. $\delta^{13}C_{DIC}$ Versus Bulk Soil Conductivity Showing Isotopic Separation for Groundwater Samples and the Major Groupings.

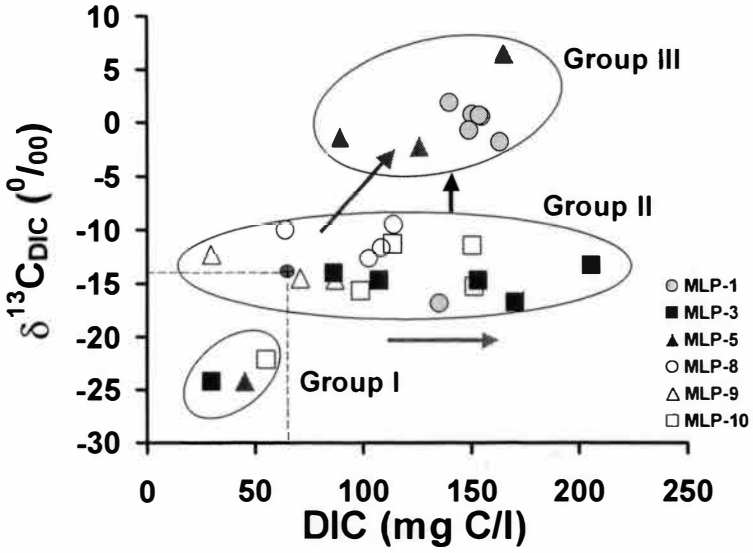

Figure 8. $\delta^{13}C_{DIC}$ Versus DIC. Arrows Show the Direction of Groundwater DIC Evolution. Groupings Are Similar to Those in Figure 7. Representative Uncontaminated Groundwater From SW Michigan Plots Within Group II.

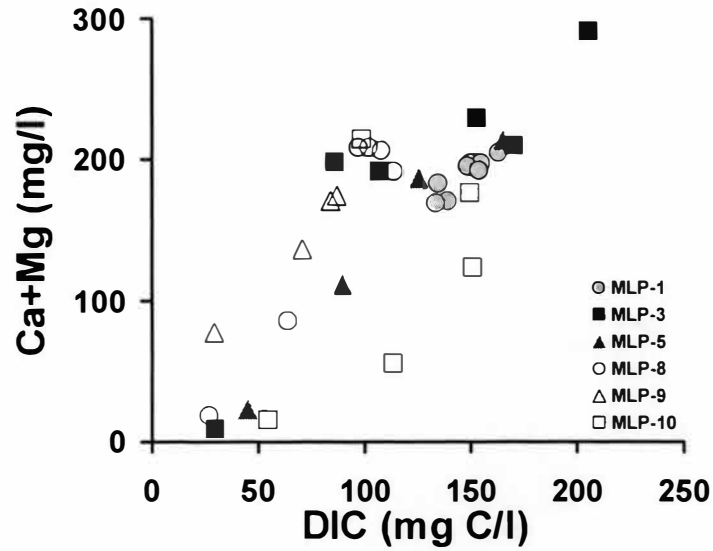

Figure 9. Ca+Mg Versus DIC for Groundwater for the Background Location (MLP-9), for Locations With Residual and Dissolved Phase Hydrocarbons (MLP-3 and MLP-10), and for Locations With Residual, Dissolved, and Free Phase Hydrocarbons (MLP-1, MLP-5, and MLP-8)

References

Archie, G. E., 1942. The electrical resistivity log as an aid in determining some reservoir characteristics. Transactions of the American Institute of Mining, Metallurgical and Petroleum Engineers, 146: 54-62.

Atekwana, E. A., Sauck, W. A. and Werkema, D. D., 2000. Investigations of geoelectrical signatures at a hydrocarbon contaminated site. J. Appl. Geophys., 44: 167-180.

Atekwana, E. A., Sauck, W. A., Abdel Aal, G.Z. and Werkema, D. D., 2002. Geophysical investigation of vadose zone conductivity anomalies at a hydrocarbon contaminated site: implications for the assessment of intrinsic bioremediation: In press, J. Environ. Eng. Geophys.

Atekwana E. A. and Krishnamurthy, R. V., 1998. Seasonal variations of dissolved inorganic carbon and $\delta^{13}C$ of surface waters: Application of a modified gas evolution technique. J. Hydrol., 205: 265-278.

Bennett, P. C., Siegel, D. E., Baedecker, M. J. and Hult, M. F., 1993. Crude oil in a shallow sand and gravel aquifer - I. Hydrogeology and Inorganic Geochemistry. Appl. Geochem., 8: 529-549.

Bennett, P.C., Hiebert, F. K. and Joo Choi, W., 1996. Microbial colonization and weathering of silicates in a petroleum-contaminated groundwater. Chemical Geology, 132: 45-53.

Bekins, B., Rittmann, B. E. and MacDonald, J. A., 2001. Natural attenuation strategy for groundwater cleanup focuses on demonstrating cause and effect: EOS, Transactions American Geophysical Union, 82(5), 53: Jan. 30, 2001.

Cassidy, D. P., Werkema, D. D., Sauck, W. A., Atekwana, E. A., Rossbach, S. and Duris, J., 2001. The effects of LNAPL biodegradation products on electrical conductivity measurements. J. Environ. Eng. Geophys., 6: 47-52.

Cassidy, D. P, Hudak, A. J., Werkema, D. D., Atekwana, E. A., Rossbach, S., Duris, J. W., Atekwana, E. A. and Sauck, W. A., 2002. In-situ Rhamnolipid production at an abandoned petroleum refinery by *Pseudomonas aeruginosa*. (In Press), J. Soil and Sed. Cont.

Conrad, M. E., Daley, P. F., Fischer, M. L., Buchanan, B. B., Leighton, T. and Kashgarian, M., 1997. Combined $\delta^{14}C$ and $\delta^{13}C$ monitoring of in-situ biodegradation of petroleum hydrocarbons. Environ. Sci. Technol., 31: 1463-1469.

Cozzarelli, I. M., Eganhouse, R. P. and Baedecker, M. J., 1990. Transformation of monoaromatic hydrocarbons to organic acids in anoxic groundwater environment. Environ: Geol. Water Sci., 16: 135-141.

Cozzarelli, I. M., Baedecker, M. J., Eganhouse, R. P. and Goerlitz, D. F., 1994. The geochemical evolution of low-molecular-weight organic acids derived from the degradation of petroleum contaminants in groundwater. Geochim. Cosmochim. Acta., 58: 863-877.

Cozzarelli, I. M., Bekins, B. A., Baedecker, M. J., Aiken, G. R., Eganhouse, R. P. and Tuccillo, M. E., 2001. Progression of natural attenuation processes at a crude oil spill site: I. Geochemical evolution of the plume. Jour. Cont. Hydrol., 53: 369-385.

Dell Engineering, 1992. Remedial Action Plan for Crystal Refining Company, 801 North Williams Street, Carson City, MI. Report DEI No. 921660, Holland, MI.

Duris, J. W., Werkema, D. D., Atekwana, E. A., Eversole, R., Beuving, L. and Rossbach, S., 2000. Microbial communities and their effects on silica structure and geophysical properties in hydrocarbon impacted sediments. Geological Society of America Program with Abstracts, 32: A-190.

Grossman, E.A., 1997. Stable carbon isotopes as indicators of microbial activities in aquifers. In: C. J. Hurst (Editor), Manual of Environmental Microbiology (pp. 565-576). Washington, DC: ASM Press.

Hach Company, 1992. Digital Titrator Model 16900-01 Manual.

Hach Company, 2000. Colorimetrer Procedures Manual.

Hem, J. D., 1985. Study and interpretation of the chemical characteristics of natural water, 3rd Edition. U.S. Geological Survey Water-Supply Paper 2254, 263 p.

Herczeg, A. L., Richardson, S. B. and Dillon, P. J., 1991. Importance of methanogenesis for organic carbon mineralization in groundwater contaminated by liquid effluent, South Australia. Appl. Geochem., 6: 533-542.

Herczeg, A. L. and Edmunds, W.M., 2000. Inorganic ions as tracers. In: P. Cook and A. L. Herczeg (Editors), Environmental tracers in subsurface hydrology (pp. 31-77). Boston: Kluwer Academic Publishers.

Hiebert, F. K. and Bennett, P. C., 1992. Microbial control of silicate weathering in organic-rich groundwater. Science, 258: 278-281.

Knight, R., 2001. Ground penetrating radar for environmental applications. Annual Review Earth and Planetary Science, 29: 229-225.

Knight, R. J. and Endres, A., 1990. A new concept in modeling the dielectric response of sandstones: Defining a wetted rock and bulk water system. Geophysics, 55: 586-594.

Lesmes, D. P. and Morgan, F. D., 2001. Dielectric spectroscopy of sedimentary rocks. J. Geophysical Research, 106: 13329-13346.

Legall, F. D., 2002. Geochemical and isotopic evidence for high conductivities in a shallow aquifer contaminated with hydrocarbons. Unpublished PhD Thesis, Western Michigan University, Kalamazoo, MI.

Mazác, O., Benes, L., Landa, I. and Maskova, A., 1990. Determination of the extent of oil contamination in groundwater by geoelectrical methods, S.H. Ward (Editor). Geotech. Environ. Geophys., 2: 107-112.

McMahon, P B. and Chapelle, F H., 1991. Geochemistry of dissolved inorganic carbon in a Coastal Plain aquifer. 2. Modeling carbon sources, sinks and $\delta^{13}C$ evolution. J. Hydrol., 127: 109-135.

McMahon, P. B. Vroblesky, D. A., Bradley, P. M., Chapelle, F. H. and Gullet, C. D., 1995. Evidence for enhanced mineral dissolution in organic acid-rich shallow ground water. Ground Water, 33: 207-216.

Nascimento, C., Atekwana, E.A. and Krishnamurthy, R.V., 1997. Concentrations and isotope ratios of dissolved inorganic carbon in denitrifying environments. Geophysical. Research Letters, 26(12): 1511-1514.

Routh, J., Grossman, E. L., Ulrich, G. A. and Suflita, J. M., 2001. Volatile organic acids and microbial processes in the Yegua formation, east-central Texas. Applied Geochemistry, 16: 183-195.

Sauck, W.A., Atekwana, E.A. and Nash, M.S., 1998. Elevated conductivities associated with an LNAPL plume imaged by integrated geophysical techniques. J. Environ. Eng. Geophys., 2-3: 203-212.

Sauck, W. A., 2000. A conceptual model for the geoelectrical response of LNAPL plumes in granular sediments. J. Appl. Geophys., 44: 151-165.

Scholl, M. A. and Harvey, R. W., 1992. Laboratory investigations on the role of sediment surface and groundwater chemistry in transport of bacteria through a contaminated sandy aquifer. Environ. Sci. Technol., 26: 1410-1417.

Snell Environmental Group, 1994. I. Technical Memorandum Task 1B - IRAP Evaluation, Crystal Refinery, 801 N. Williams Street, Carson City, Michigan. MERA ID #59003.

Stumm, W., 1992. Chemistry of the solid-water interface: Processes at the mineral-water and particle-water interface in natural systems. New York: John Wiley and Sons, 428 p.

Stumm, W. and Morgan, J. J., 1995. Aquatic chemistry: Chemical equilibria and rates in natural waters, 3rd edition. New York: John Wiley and Sons, 1022 p.

Ullman, W. J. and Welch, S. A., 2002. Organic ligands and feldspar dissolution. In R. Hellmann and S. A. Ward (Editors), Water-rock interactions, ore-deposits, and environmental geochemistry-A tribute to David A. Crerar. The Geochemical Society Special Publication No. 7, 2002.

Wasserman, E. and Felmy, A. R., 2000. Modeling the electrical double layer on microbial surfaces: Equilibrium and non-equilibrium treatments. In: From atoms to organisms (and back): Rates and mechanisms of geochemical processes. Abstracts Geosciences Research Program, Office of Science, Department of Energy, p. 21.

Werkema D. D., Atekwana, E. A., Sauck, W. A., Rossbach, S. and Duris, J., 2000. Vertical distribution of microbial abundances and apparent resistivity at an LNAPL spill site. Proceedings of the Symposium on the Application of Geophysics to Engineering and Environmental Problems (SAGEEP), Arlington Virginia, pp. 669-678.

Werkema D. D., 2002. Geoelectrical Response of an Aged LNAPL Plume. Implications for Monitoring Natural Attenuation. Unpublished Ph.D Thesis, Western Michigan University, Kalamazoo, MI.

Wildenschild, D., Roberts, J. J. and Carlberg, E. D., 1999. On the relationship between microstructure and electrical and hydraulic properties of sand-clay mixtures. Open File Report, Experimental Geophysics Group, U.S. Dept. of Energy, Lawrence Livermore National Laboratory, UCRL-ID-136122, 15 p.

CHAPTER IV

CONCLUSION

Geochemical and geophysical studies have rarely been coordinated at hydrocarbon-contaminated sites. However, the results of this study confirm that integrating the results from high resolution (~2 cm interval) bulk conductivity measurements with detailed groundwater monitoring from closely spaced (~30 cm interval) geochemical sampling can provide valuable information on the spatial and vertical variability of geochemical processes governing plume behavior and development that cannot be achieved by geochemical sampling in conventional monitoring wells.

This study demonstrated that information collected from VRPs can be used to successfully guide the placement of multi-level piezometers within anomalously conductive zones and the geochemical data gathered can be used to effectively monitor intrinsic biremediation of the hydrocarbon plume. Zones of high conductivities identified in the geophysical data were targeted for further evaluation using closely spaced geochemical sampling. Through this process the arbitrary selection of subsurface intervals for sampling was eliminated. Moreover, the results obtained by simultaneous examination of soil conductivity and groundwater chemistry along vertical profiles lead to a better understanding of the dynamics that interrelate biogeochemical, geological, and hydrological processes of subsurface hydrocarbon-impacted media and how these interrelations translate into measurable changes in the geophysical

signatures.

The existence of steep vertical conductivity and chemical gradients that are known to accompany geochemical reactions in the subsurface (Ronen et al., 1987; Smith et al. 1991a) were confirmed in the vertical profiles. These gradients occur over intervals that are <50 cm thick, therefore, conventional groundwater monitoring wells that are commonly used for monitoring intrinsic bioremediation that are typically screened over a large interval (> 1m) would have been unable to provide the resolution to characterize the subsurface processes related to the observed gradients (Smith et al., 1991a). The combined use of the VRPs and closely spaced vertical geochemical sampling outlined in this study has proved to be effective in identifying zones with steep vertical conductivity and concentration gradients and for corroborating interpretations of the chemical and microbial processes occurring in contaminated aquifers.

The results of this study demonstrate conclusively the link between high bulk conductivities measured in contaminated soils and subsurface redox zonation related to hydrocarbon biodegradation. Considerable vertical variability was observed in the subsurface distribution of redox processes with redox reactions occurring in zones < 50 cm thick. Resolution of narrower intervals is apparently possible using smaller vertical sampling intervals. The observed variability in the subsurface distribution of redox processes suggests that the generally accepted models of well demarcated redox zones developed for numerous contaminated sites based on bulk groundwater samples obtained from individual wells are far too simplistic. Furthermore, this study

has firmly established that elevated soil conductivity measurements in hydrocarbon contaminated soils are due to increased ion concentration in the pore water resulting from enhanced mineral dissolution by inorganic and organic acids produced during microbial hydrocarbon degradation.

These observations have significant implications for future efforts aimed at monitoring natural attenuation of hydrocarbons in the subsurface. Because of the inherent uncertainty associated the spatial and vertical distribution of contaminants in the subsurface, placement of sample collection points is a critical aspect of effective site characterization, validation monitoring, and long term monitoring strategies (Wiedemeier and Haas, 2002). In this regard, data from vertical resistivity surveys can be used to guide the placement of subsurface sampling locations and can provide proxy information of expected chemical gradients in the dynamic conditions encountered in the groundwater environment, especially within the unsaturated zone where it is often difficult to sample. In the absence of geochemical data, the bulk conductivity measurements can identify discrete zones where physical and chemical changes are occurring and therefore can independently serve as a proxy for monitoring the development or attenuation of contaminant plumes because of the demonstrated link between changes in the bulk conductivity signature and geochemical changes related to in-situ chemical and microbial processes.

Geoscientists can effectively combine the geophysical and geochemical techniques used in this study to gain a better understanding of the dynamics that interrelate biological, chemical, geological, and hydrological processes in subsurface

LNAPL perturbed media. The collective use of these techniques can translate to significant cost savings by reducing the number of wells required for monitoring and sampling as well as the sampling frequency, which in turn will result in lower analytical costs. To date, the potential of geophysical information for use in contaminant delineation, monitoring, and remediation in the subsurface has still not been fully exploited.

References

Ronen, D., Magaritz, M., Gvirtzman, H. and Garner, W., 1987. Microscale chemical heterogeneity in groundwater. J. Hydrol., 92: 173-178.

Smith, R.L, Harvey, R.W. and LeBlanc, D.R., 1991a. Importance of closely spaced vertical sampling in delineating chemical and microbial gradients in groundwater studies. Jour. Cont. Hydrol., 7: 285-300.

Wiedemeier, T.H. and Haas, P.E., 2002. Designing monitoring programs to effectively evaluate the performance of natural attenuation. Ground Water Monitoring and Remediation, 22(3): 124-134.